


NGU Report 2012.034
ARCTIC CHRONOLOGY REPORT

Rapport nr.: 2012.034		ISSN 0800-3416	Gradering: Åpen
Tittel: ARCTIC CHRONOLOGY REPORT			
Forfatter: Knies, J., Andreassen, K., Husum, K., Mattingsdal, R., Fabian, K., Grøsfjeld, K.		Oppdragsgiver: Det Norske Oljeselskap, Statoil ASA, BG Norge	
Fylke:		Kommune:	
Kartblad (M=1:250.000)		Kartbladnr. og -navn (M=1:50.000)	
Forekomstens navn og koordinater:		Sidetall: 43 Kartbilag:	Pris: 155,-
Feltarbeid utført: 2008, 2009, 2010	Rapportdato: 30.04.2012	Prosjektnr.: 327000	Ansvarlig: 
Sammendrag:			
<p>Our major goal improving the chronostratigraphic framework for ODP site 910 and 911 from the marginal Arctic Ocean was successfully achieved. We have agreed on a new age model for both sites. We do not see any evidence for a hiatus in the sections. The collection of new high-resolution seismic data across the Yermak Plateau allows a perfect correlation between the sites. Both the new biostratigraphic and paleomagnetic data support the inferences from seismic correlation that the base of Hole 911A is slightly younger (~5.3 Ma) than Hole 910C (~5.8 Ma) (Fig. 1.1). The new data indicate that the base of the boreholes is approximately 2.5 Ma older than previously assigned (see ODP Leg 151 Scientific/Initial Reports) (Fig. 1.2). All available old/new age fixpoints for both boreholes are summarized in Table 1.1.</p> <p>The new Plio-Pleistocene seismo-stratigraphic framework has been established along the western Svalbard margin between ODP site 911 on the Yermak Plateau and ODP site 986 offshore south-western Svalbard (Fig. 2.1). Although site 986 has been a key borehole for seismic stratigraphy of the western Barents Sea – Svalbard margin, a discrepancy between the biostratigraphy and the paleomagnetic/Sr-data has shed doubts about age estimates from this well. Our results now confirm the age of the main seismic reflectors R7 to 2.7 Ma, R5 to 1.5 Ma and R3 to 0.78 Ma.</p>			
Emneord:	Arctic Ocean	Yermak Plateau	
Barents Sea	Chronostratigraphy	Late Neogene	2

CONTENTS

1. EXECUTIVE SUMMARY	4
2. BACKGROUND AND OBJECTIVES	8
3. RESULTS AND DISCUSSION	9
3.1 Module 1: Biostratigraphy based on planktic and benthic foraminifera (PI: Katrine Husum, University of Tromsø)	9
3.2 Module 1: Biostratigraphy based on dinoflagellate cysts (Kari Grøsfjeld, Geological Survey of Norway)	11
3.3 Module 2: Stable oxygen and carbon isotope record of Hole 910 (PI: Jochen Knies, Geological Survey of Norway)	13
3.4 Module 2: Paleomagnetic record of Hole 910C and 911A (Karl Fabian, Geological Survey of Norway)	18
3.5 Module 3: Seismo-stratigraphic framework of the western Svalbard/Barents Sea margin (PI: Karin Andreassen, University of Tromsø).....	22
4. A NEW CONSISTENT AGE MODEL FOR THE YERMAK PLATEAU.....	26
5. PALEOCLIMATIC IMPLICATIONS	29
6. MAIN CONCLUSIONS	39
6.1 Stratigraphy:	39
6.2 Environment:	39
6.3 Hydrocarbons.....	40
7. OUTLOOK: CORRELATION POTENTIAL TOWARDS THE SW BARENTS SEA..	40
8. REFERENCES	41

ARCTIC CHRONOLOGY REPORT

1. EXECUTIVE SUMMARY

Our major goal improving the chronostratigraphic framework for ODP site 910 and 911 from the marginal Arctic Ocean was successfully achieved. We have agreed on a new age model for both sites. We do not see any evidence for a hiatus in the sections. The collection of new high-resolution seismic data across the Yermak Plateau allows a perfect correlation between the sites. Both the new biostratigraphic and paleomagnetic data support the inferences from seismic correlation that the base of Hole 911A is slightly younger (~**5.3 Ma**) than Hole 910C (~**5.8 Ma**) (Fig. 1.1). The new data indicate that the base of the boreholes is approximately 2.5 Ma older than previously assigned (see ODP Leg 151 Scientific/Initial Reports) (Fig. 1.2). All available old/new age fixpoints for both boreholes are summarized in Table 1.1.

The new Plio-Pleistocene seismo-stratigraphic framework has been established along the western Svalbard margin between ODP site 911 on the Yermak Plateau and ODP site 986 offshore south-western Svalbard (Fig. 2.1). Although site 986 has been a key borehole for seismic stratigraphy of the western Barents Sea – Svalbard margin, a discrepancy between the biostratigraphy and the paleomagnetic/Sr-data has shed doubts about age estimates from this well. Our results now confirm the age of the main seismic reflectors R7 to **2.7 Ma**, R5 to **1.5 Ma** and R3 to **0.78 Ma**.

The ultimate correlation towards the southwestern Barents Sea is hampered by the lack of access to available seismic data from Russia (MAGE). During course of NFR Petromaks project “GlaciBar”, the data may be available after all.

The depositional environment inferred from new seismic and borehole data can be classified into three phases: (1) Prior to 2.7 Ma, contouritic deposits dominate the system. An eastward migrating system associated with the prevalence of the northernmost branch of the North Atlantic Drift is inferred. (2) At 2.7 Ma, an abrupt rise in IRD together with the onset of Isfjorden and Sjubrebanken through mouth fans mark the onset of the Northern Hemisphere Glaciation (NHG) (3) At 1.5 Ma, a prominent switch of depocenter from Sjubrebanken to Kongsfjorden fan and detection of iceberg ploughmarks on eastern and western side of the Yermak Plateau indicate both a change in sediment source and style of glaciations in the Svalbard/Barents Sea. The latter is consistent with observations for the entire western Barents Sea suggesting the establishment of large-scale (late Quaternary style) glaciations and glacial erosion in the entire Barents Sea since 1.5 Ma.

Prior to 2.7 Ma, planktic and benthic foraminifera indicate subpolar – polar conditions. In addition the benthic foraminifera are typical for outer shelf – upper slope assemblages. The build-up of contourites suggests sediment transport predominantly through northward flowing water masses, e.g. the North Atlantic Drift. In addition, large amount of organic debris including fresh plant remains associated with pulses of fine sand indicate a near-coastal environment and (glacial) fluvial processes that influenced the Yermak Plateau during the late Miocene-early Pliocene (~5.8-4.4 Ma). The almost continuous record of fresh water algae demonstrates a proximity to the coast and river outflow during this interval; however, release during melting of sea ice cannot be excluded. A switch in clay mineral assemblages (more illite) coupled to a distinct drop in fine sand mark climate deterioration during the early Pliocene. More frequent pulses of (glacially-derived) Ti-rich sediments from northern

Svalbard since ~4 Ma resemble a glacial-interglacial climate pattern typical for the late Quaternary.

A number of hydrocarbon indications are observed on the Yermak Plateau. Most prominent are the crestal parts of the eastward migrating contourrite where bright spots are associated with masking below. Other bright spots are related to free gas, migrating up along the faults and permeable layers, accumulating in the structural traps of the anticlines. There, we also observe flat spots. A bottom simulating reflector (BSR) at the base of the modeled gas hydrate stability zone (GHSZ) is tentatively observed at one location. Migration of gaseous hydrocarbons occurred prior to the intensification of the Northern Hemisphere Glaciations (~2.7 Ma) as indicated by high-amplitude reflections, corroborating the occurrence of greigite mineralization and stable carbon isotope excursions in planktic/benthic foraminifera. The data indicate that Pleistocene erosion and uplift in the Barents Sea region had probably only minor effects on reservoir leakages than previously thought.

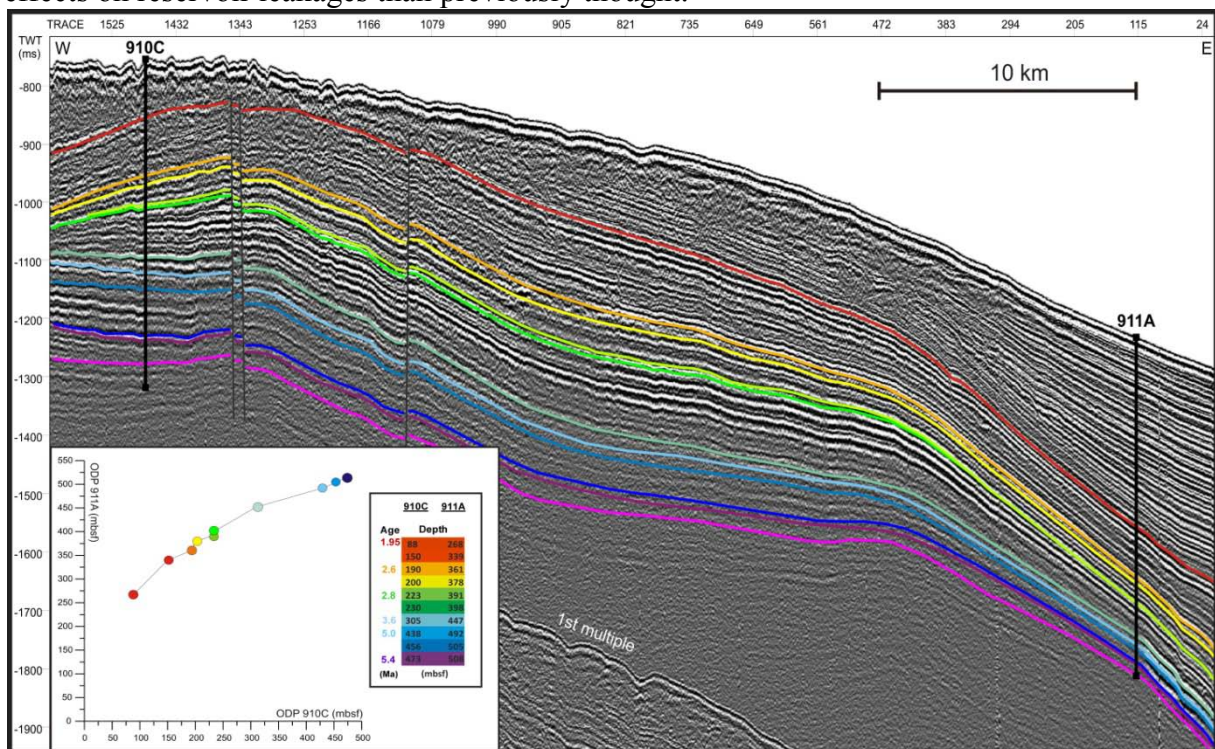


Figure 1.1 Seismic reflection profile and correlation between ODP Sites 910 and 911. Depth correlation between both sites and respective ages are shown in the inset.

Chronology 2009/2012

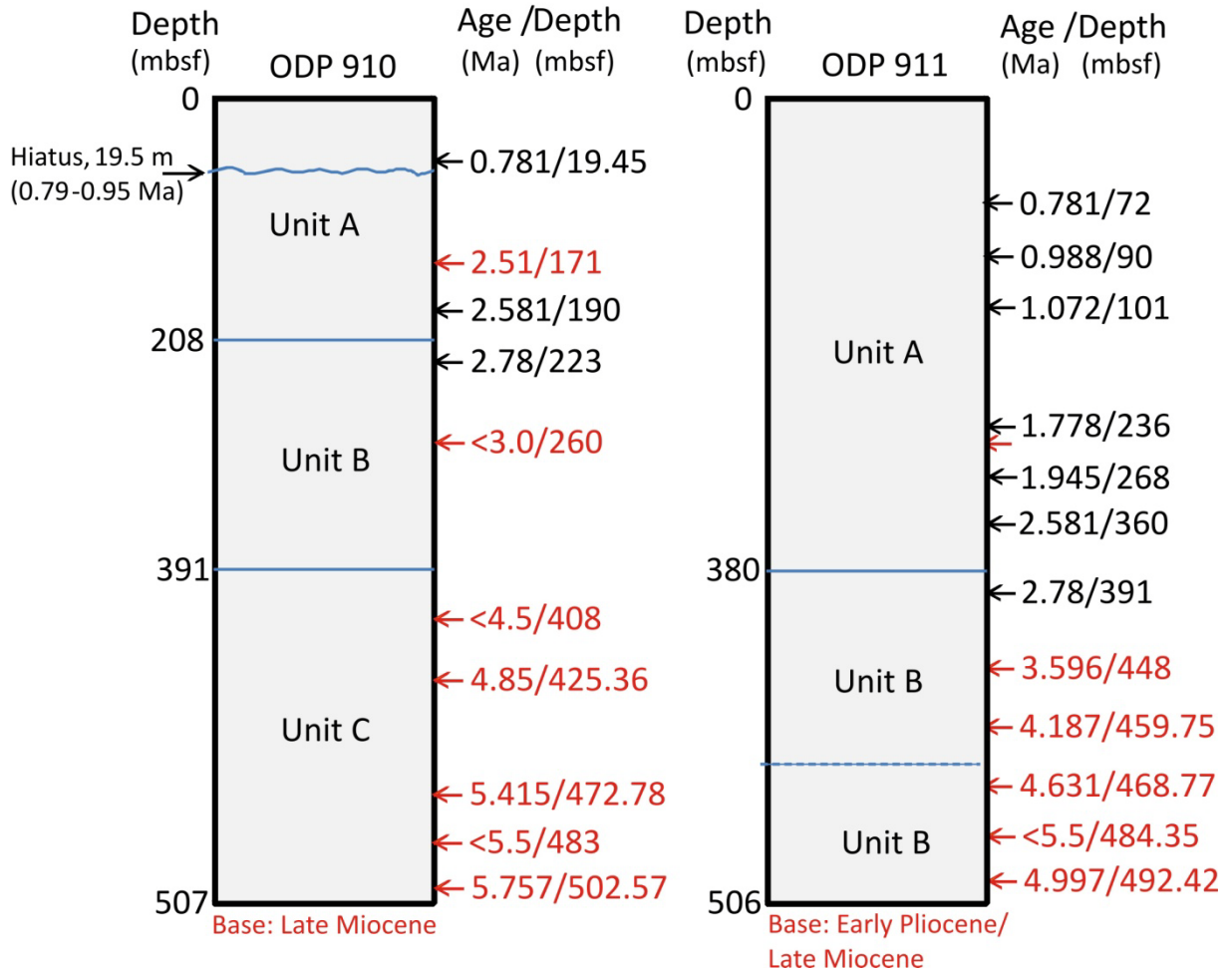


Figure 1.2 Old and new chronostratigraphic framework of ODP Sites 910 and 911. Numbers in black indicate the age model prior to project Start. Red numbers are based on 1st (paleomagnetic/biostratigraphic) and 2nd (marine isotope stages) order age fixpoints.

(A)

ODP Hole 910C, 1st order fixpoint						
Depth (cm)	Depth (mbsf)	Age (years)	Age (years *1000)	Sedimentationrate (cm/1000 years)	Source/Datums	Reference
>15190	>151.9	2410000	2410		LO <i>N. atlantica</i>	Spiegler 1996
19000	190	2581000	2581	22.28	Paleomag (M/G boundary)	Lourens et al. 2005
22300	223	2780000	2780	16.58	Biostrat. "Datum A"	Sato & Kameo 1996
26000	260	<3000000	3000	16.82	Biostrat. HO, <i>L. crista</i>	de Schepper & Head 2008
40800	408	<4500000	4500	9.87	Biostrat. FO, <i>S. islandensis</i>	Verhoeven et al. 2011
48350	483.5	<5500000	5500	7.55	Biostrat. FO, <i>L. crista</i>	de Schepper & Head 2008

ODP Hole 911A, 1st order fixpoint						
Depth (cm)	Depth (mbsf)	Age (years)	Age (years*1000)	Sedimentationrate (cm/1000 years)	Source/Datums	Reference
0	0	0	0			
7200	72	781000	781	9.22	Paleomag (B/M)	Lourens et al. 2005
9000	90	988000	988	8.70	Paleomag (Jaramillo Top)	Lourens et al. 2005
10100	101	1072000	1072	13.10	Paleomag (Jaramillo Base)	Lourens et al. 2005
23600	236	1778000	1778	19.12	Paleomag (Olduvai Top)	Lourens et al. 2005
26800	268	1945000	1945	19.16	Paleomag (Olduvai Base)	Lourens et al. 2005
36133	361.33	2581000	2581	14.67	Paleomag (M/G)	Lourens et al. 2005
39190	391.9	2780000	2780	15.36	Biostrat. "Datum A"	Sato & Kameo 1996
44700	447	3596000	3596	6.75	Paleomag (G/G)	Lourens et al. 2005
45975	459.75	4187000	4187	2.16	Paleomag (Cochiti Top)	Lourens et al. 2005
46877	468.77	4631000	4631	2.03	Paleomag (Nunivak Base)	Lourens et al. 2005
48435	484.35	<5500000	<5500		Biostrat. FO <i>L. crista</i>	de Schepper & Head 2008
49242	492.42	4997000	4997	6.46	Paleomag (Thvera Top)	Lourens et al. 2005

(B)

ODP Hole 910C, 2nd order fixpoints						
Depth (cm)	Depth (mbsf)	Age (years)	Age (years *1000)	Sedimentationrate (cm/1000 years)	Source/Datums	Reference
17100	171	2510000	2510		Marine Isotope Stage 100, Top	Lisiecki & Raymo 2005
17568	175.7	2540000	2540	15.60	Marine Isotope Stage 100, Base	Lisiecki & Raymo 2005
42536	425.36	4854000	4854	10.79	Marine Isotope Stage event Si4	Hodell et al. 2001
47278	472.78	5415000	5415	8.45	Marine Isotope Stage d18O light event at 5.415 Ma	Zachos et al. 2001
50257	502.57	5757000	5757	8.71	Marine Isotope Stage event TG20	Hodell et al. 2001

ODP Hole 911A, 2nd order fixpoints						
Depth (cm)	Depth (mbsf)	Age (years)	Age (years*1000)	Sedimentationrate (cm/1000 years)	Source/Datums	Reference
42251	422.51	3290000	3290		M2 glaciation, IRD peak	Lisiecki & Raymo 2005
50293	502.93	5262000	5262	4.08	Correlation Point XRF, 910	
50545	505.45	5317000	5317	4.58	Correlation Point XRF, 910	

(C)

Fine tuning of age model above against LR04 global stack						
Depth (cm)	Depth (mbsf)	Age before tuning	Age after tuning	Source/Datums	Reference	
17357	173.57	2523.4	2520.9	MIS 100		
38027	380.27	4382.7	4361.0 11.23	MIS CN4	Lisiecki & Raymo 2005	
38438	384.38	4425.7	4416.6 7.39	MIS CN6	Lisiecki & Raymo 2005	
39560	395.6	4543.0	4532.3 9.69	MIS N4	Lisiecki & Raymo 2005	
40304	403.04	4620.7	4611.1 9.45	MIS N8	Lisiecki & Raymo 2005	
41646	416.46	4761.0	4771.2 8.38	NS6	Lisiecki & Raymo 2005	
42536	425.36	4854.0	4849.4 11.38	Si4	Lisiecki & Raymo 2005	
42837	428.37	4889.6	4894.2 6.71	Si6	Lisiecki & Raymo 2005	
43279	432.79	4941.9	4942.4 9.17	ST2	Lisiecki & Raymo 2005	
43580	435.8	4977.5	4980.9 7.83	ST4	Lisiecki & Raymo 2005	
44607	446.07	5099.0	5104.6 8.30	T6	Lisiecki & Raymo 2005	
45277	452.77	5178.3	5175.9 9.40	T8	Lisiecki & Raymo 2005	

Tabel 1.1 (A) 1st order fixpoints, (B), 2nd order fixpoints of Hole 911A and Hole 910C. (C) Tuning of Hole 910C stable isotope record against LR04 (Lisiecki & Raymo 2005).

2. BACKGROUND AND OBJECTIVES

As an important contribution to future planned exploration of Arctic frontiers including the Barents Sea, we have worked out a refined stratigraphic framework for the Barents Sea by working on existing ODP sites 910 and 911 from the marginal Arctic Ocean. We have chosen the Yermak Plateau – the Atlantic/Arctic Ocean gateway – as key area for our study because, (1) here, rather than along the western Barents Sea or even the central Arctic Ocean, carbonate bearing sequences permit establishment of a relatively continuous stable oxygen isotope and foraminiferal stratigraphy, which is still the prerequisite for any subsequent application of chronological approaches, and (2) the site is characterized by a dynamic coupling between the northernmost branch of the Gulf Stream and the Arctic Ocean.

We have selected two locations of high priority recovered during ODP Leg 151 (Hole 910C, 911A) (Figure 2.1). At these sites, we have established a new reference stratigraphy for the last ~6 Ma. Coupled to new high-resolution seismic data, the improved stratigraphic framework has been integrated into an updated seismostratigraphic network for the western Barents Sea margin. Throughout the project period we addressed three tasks defined below:

- 1) Consistent stratigraphic framework for Plio-Pleistocene sediment sequences,
- 2) Expanded knowledge on coupled ice dynamics and paleoceanographic changes during the Plio-Pleistocene
- 3) Improved spatio-temporal information on glacial erosion in the Barents Sea during the Plio-Pleistocene.

The project was divided in three different modules:

Module 1 provided a detailed biostratigraphy, lithostratigraphy (IRD) and chronostratigraphy based on benthic and planktic foraminifera as well as dinoflagellate cysts.

Module 2 provided a new planktonic and benthic stable isotope record for Hole 910C as well as a complete paleomagnetic record for both boreholes.

Module 3 integrated the new reference stratigraphy with a new seismo-stratigraphic framework of the western Svalbard/Barents Sea continental margin and shelf. New and available 2D seismic data, acquired by academic institutions (mainly UiT) and the Norwegian Petroleum Directorate (NPD) were used.

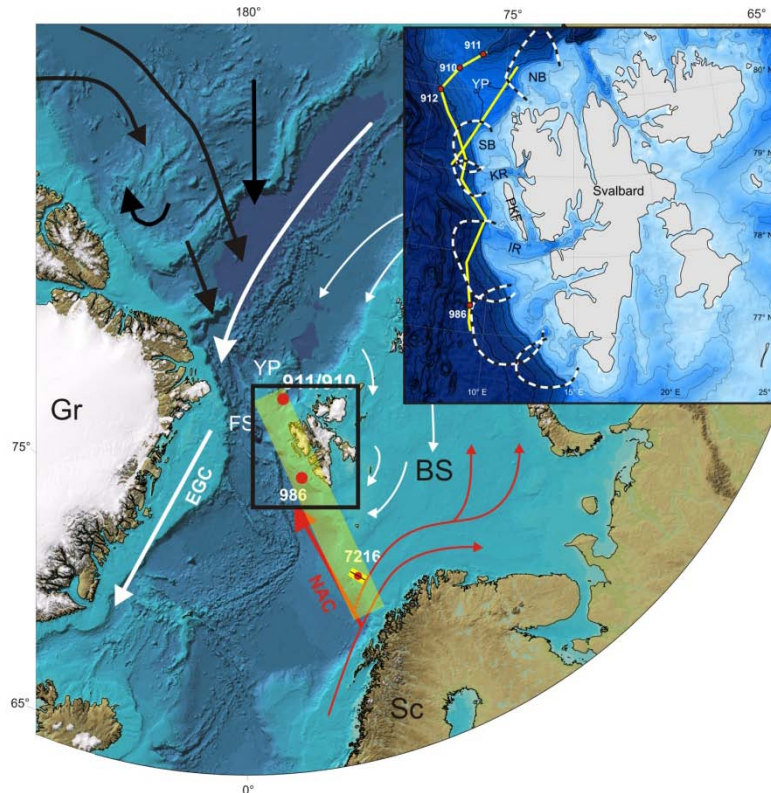


Figure 2.1 Study area (yellow) and location of key boreholes. Arrows indicate surface ocean circulation (red: warm; white/black: cold). Inset shows location of ODP sites, discussed seismic sections, and Quaternary fans along the Western Svalbard margin (stippled black and white outlines). YP = Yermak Plateau, NB = Norskebanken, SB = Sjubrebanken, KR = Kongsfjordrenna, IR = Isfjordrenna.

3. RESULTS AND DISCUSSION

3.1 Module 1: Biostratigraphy based on planktic and benthic foraminifera (PI: Katrine Husum, University of Tromsø)

High latitude foraminiferal assemblages are of low diversity, and as such biostratigraphic datums are infrequent. However, preliminary ages were assigned using Neogene planktic biostratigraphic zonation from the North Atlantic (Weaver and Clement, 1987; Spezzaferri, 1998) for the Miocene and Pliocene from the Yermak Plateau. Planktic foraminiferal taxonomy largely follows that of Kennett and Srinivasan (1983). The benthic taxonomy follows the definitions by Loeblich and Tappan (1988). The Neogene timescale correlated to magnetostratigraphy as defined by Lourens et al. (2004) was applied in this study.

The analysis of the foraminiferal assemblages of Hole 910C show both benthic and planktic foraminifera (Fig. 3.1.1). The occurrence of the planktic foraminiferal species *Neogloboquadrina atlantica* (sin) sets the base of the borehole in a time frame from late Miocene to the end of Pliocene (Kennett and Srinivasan 1983). Late Miocene starts ~11.6 Ma, and the end of Pliocene was previously defined as ~1.8 Ma (Ogg et al. 2008, ICS 2010). The benthic foraminifera *Cibicides grossa* was also found at the base of Hole 910C, which would suggest a Pliocene age for the base of Hole 910C (e.g. Feyling-Hanssen 1986; King 1983). However, this is a benthic foraminiferal species meaning its distribution is very influenced by bathymetric changes, and biostratigraphic events may be regionally diachronous. It has

recently been demonstrated that the last occurrence of *C. grossa* is diachronous, and this event is younger (Pleistocene) than previously defined (Anthonissen 2008). Other investigations have also reported an older age for the first occurrence of *C. grossa*. van Voorthuysen (1950) identified the first occurrence of *C. grossa* in Middle Miocene deposits from the Netherlands. Further north at the Vøring Plateau in the Norwegian Sea the first occurrence of *C. grossa* was observed in late Middle Miocene deposits (Eidvin and Rundberg 2001, Eidvin pers. com.) meaning that the base of Hole 910C may be late Miocene .

In Hole 911A both planktic and benthic foraminifera were found (Fig. 3.1.2). The occurrence of *Neogloboquadrina atlantica* (dex), *Neogloboquadrina atlantica* (sin) and *Cibicides grossa* place the investigated interval of Hole 911A in the time frame from Late Miocene to Pliocene as previously discussed for Hole 910C. The last occurrence of *Globigerina praebulloides* at 488.1 mbsf restricts the time frame of the lower part of Hole 911A to Late Miocene. A single specimen of *Paragloborotalia continua* at 491.40 mbsf (Spiegeler 1996) and other biostratigraphic events based on dinoflagellate cysts (see chapter 3.2) suggest that the interval around 488 mbsf must be very close to the Miocene/Pliocene transition. The upper part of Hole 911A is clearly Pliocene.

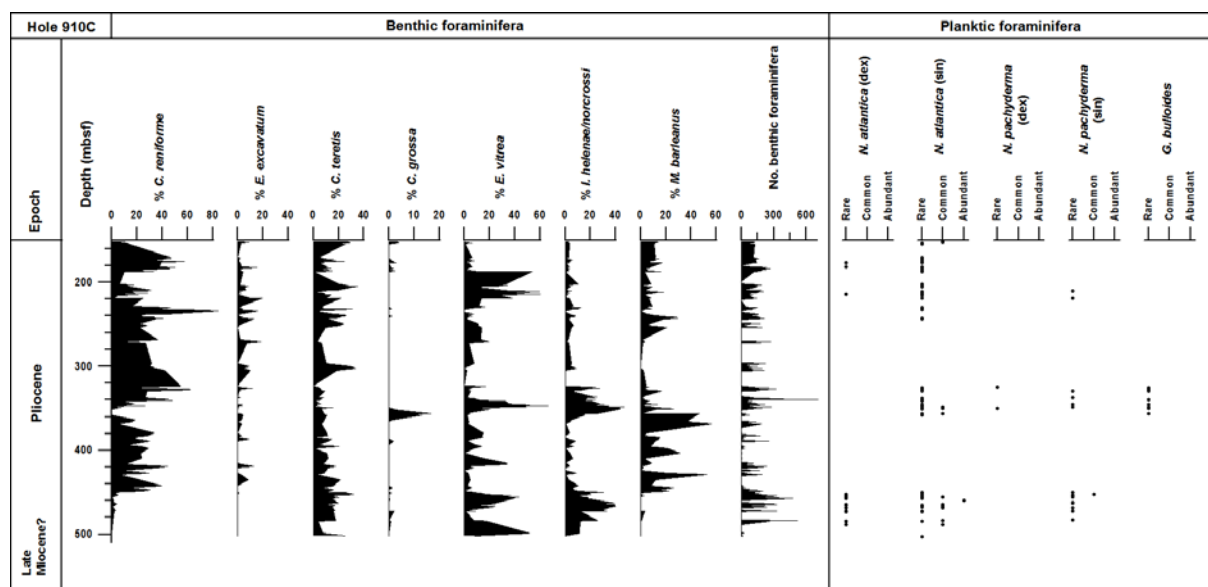


Fig. 3.1.1 Range chart of the most important biostratigraphic in addition to the most abundant species in Hole 910C. Benthic foraminifera were quantitatively analyzed and their relative abundance is shown here. Planktic foraminifera were only qualitatively analyzed. The abundance was defined as follows: A = abundant (> 10 %), C = common (5–10 %), R = rare (1–5%).

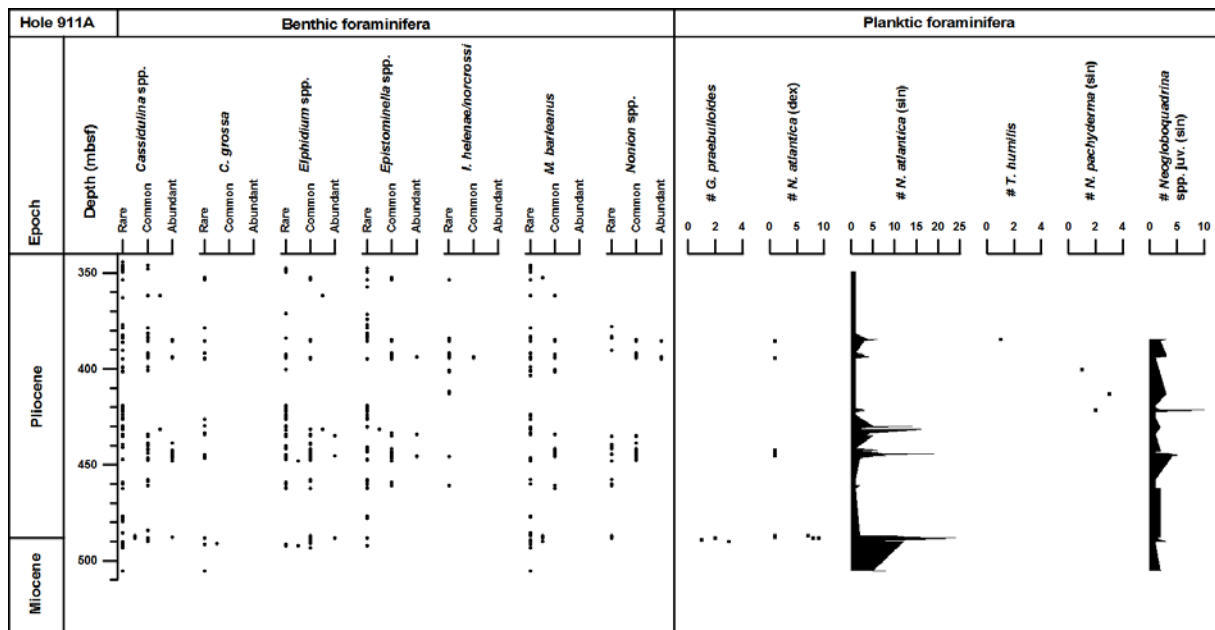


Fig. 3.1.2 Range chart of the most important biostratigraphic in addition to the most abundant species in Hole 911A. Benthic foraminifera were only qualitatively analyzed. The abundance was defined as follows: A = abundant (> 10 %), C = common (5–10 %), R = rare (1–5%). Planktic foraminifera were quantitatively analyzed. The number of specimens is shown here as the total number of specimens were too low in order to calculate robust relative abundance.

3.2 Module 1: Biostratigraphy based on dinoflagellate cysts (Kari Grøsfjeld, Geological Survey of Norway)

The sediments of Hole 911A resemble a typical Late Miocene to Pliocene sequence. However, the possibility of reworking makes definition of any Miocene-Pliocene boundary uncertain. A tentative stratigraphical Miocene - Pliocene boundary could either be placed at 1) around 489,3 mbsf, which is the highest occurrence of the Late Miocene indicator species *T. ferugnomatum*, or 2) below 503,74 mbsf, at the stratigraphically lowest level for the occurrence of *Achomosphaera andalousiensis suttonensis*. However, the sediments above 503,74 mbsf can have been deposited during the Piacenzian (late Early to early Middle Pliocene) (Fig. 3.2.1). In this case all the Late Miocene indicator species above 503,74 mbsf are possibly reworked.

In Hole 910C, the stratigraphically deepest sediments containing cysts that can provide information about the age are located at 494,45 mbsf (Fig. 3.2.2). The suggested maximum age of 13.7 – 5.5/8.8? Ma at this stratigraphic level is based on the occurrence of *Operculodinium? eirikianum eirikianum*, having LO in the Middle Miocene, and the absence of the acritarch *Lavradosphaera crista* having LO at 5.5 Ma. The oldest analyzed sediments at 505,64 mbsf in Hole 911A resemble those at 494,45 mbsf in Hole 910C. They both contain *Operculodinium? eirikianum eirikianum* and lack the acritarch *Lavradosphaera crista* and species restricted to the Pliocene.

The acritarch *Lavradosphaera. crista* was first recorded at 483,45 mbsf in Hole 910C, providing a maximum age of 5,5 Ma. A maximum age of 5.5 Ma is also indicated c. 34 m higher up in the Hole 910C at 449,96 mbsf. This is based on the co-occurrence of the acritarch species *L. crista* (LO 5.5 Ma) and *Cymatiosphaera? invaginata* (HO in Late Miocene). The Early Pliocene was recognized in Hole 910C in sediments located at 408,3 and 407,75 mbsf. This is based on *Batiacasphaera minuta/micropapillata* (HO at 3.4 Ma) at 407,75 mbsf

and the possibly reworked *Operculodinium tegillatum* (HO at 3.71 Ma) at 408,30 mbsf to 407,75 mbsf. These two species were not found in ODP Hole 911A. Moreover, the LO of *Selenopemphix islandensis* sp. nov. sensu Verhoeven and Louwye (2011) is located at 408.3 mbsf. The first and last appearance of *S. islandensis* sp. nov. in the Tjörnes region occurred at ca. 4.5 Ma and 4.2 Ma, respectively (Verhoeven and Louwye 2011).

The sediments in 910C also contain *Achomosphaera andalouensis suttonensis*. Whereas *A. andalouensis suttonensis* was recorded at several stratigraphic levels in ODP 911A, only a single specimen of this species was recorded at 408,3 mbsf in ODP 910C. Age constraints based on *A. andalouensis suttonensis* have been considered speculative as this species has so far been recorded from only a few sites (Southern England), having LO around 3.3 Ma. However, the occurrence of *A. andalouensis suttonensis* and *Batiacasphaera minuta/micropapillata* in the sediments in Hole 910C strengthen the legitimacy of *A. andalouensis suttonensis* being an Early Pliocene maximum age indicator. This species is common in the sediments at 503,74 and 503,61 mbsf in ODP Hole 911A.

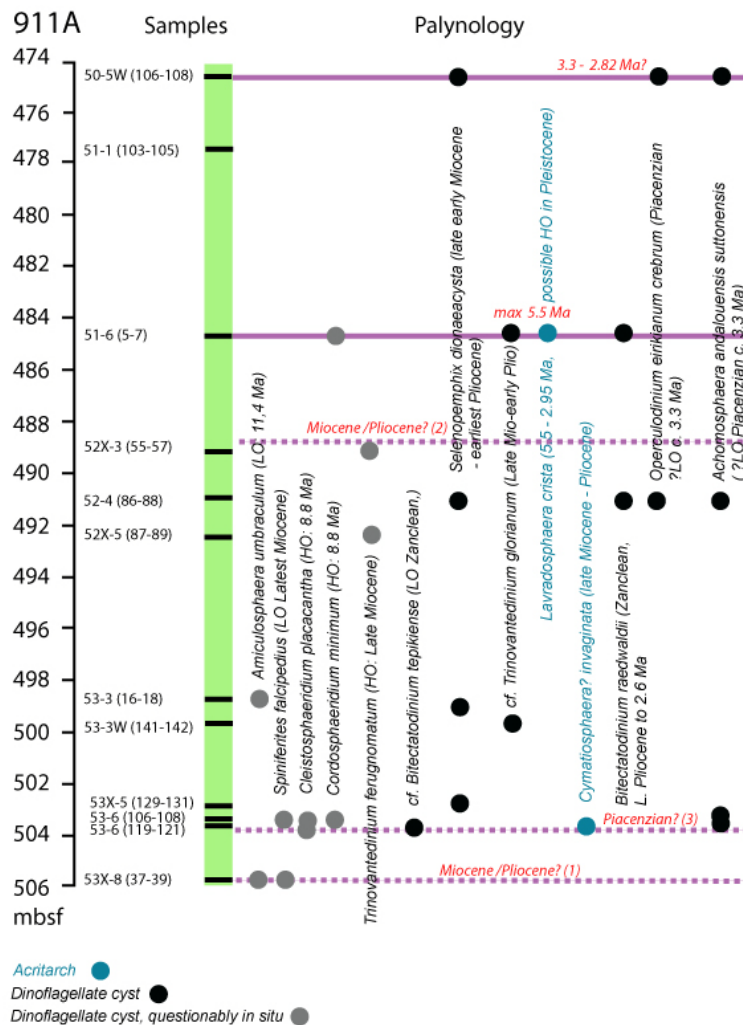


Fig. 3.2.1 Ranges of selected dinocysts and acritarch taxa in Hole 911A used for age assignment.

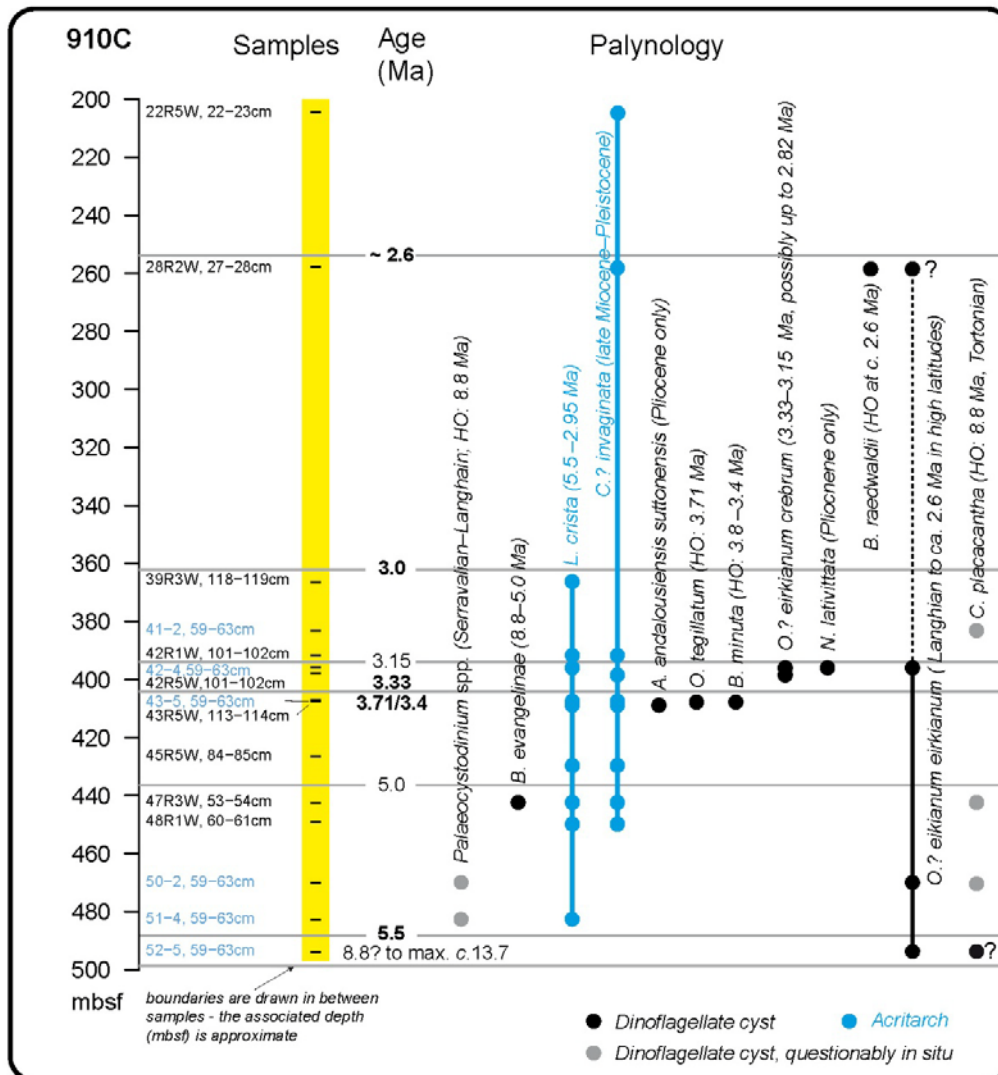


Fig. 3.2.2 Ranges of selected dinocysts and acritarch taxa in Hole 910C used for age assignment.

3.3 Module 2: Stable oxygen and carbon isotope record of Hole 910 (PI: Jochen Knies, Geological Survey of Norway)

Planktic and benthic stable isotope record of Hole 910C

For the stable isotope analyses we have continuously measured the $\delta^{18}\text{O}$ and $\delta^{13}\text{C}$ signature of the benthic foraminifera *Cassidulina teretis* and selectively *Cassidulina reniforme* in Hole 910C. In addition, planktic foraminifer *Neogloboquadrina atlantica* sin was measured if available. The work is very time consuming since ca. 50 ccm sediments were washed for ca. 10-20 foraminifera in average. ~40 percent of the samples were barren. To date, we have compiled the results of 125 benthic and 35 planktic measurements covering the time interval from ~5.8 and 2.4 Ma (Fig. 3.3.1). The gap between 2.6 and 4.0 Ma is caused by technical problems at Leibniz-Laboratory for Radiometric Dating and Isotope Research, Kiel, Germany. The results from the final batch (150 samples) are expected during the first months of 2012. Currently we prepare samples for isotopic analyses from ODP Hole 912A from the

western Yermak Plateau to fill the gap between 1.0 and 2.0 Ma. The results will be available during course of the NFR-Petromaks “GlaciBar” project.

The stable isotope record of Hole 910C exhibits distinct cycles between heavy and light oxygen isotope values with a gradual increase to heavier values between ~5.8 Ma (Base) and 2.4 Ma (Fig. 3.3.1). $\delta^{18}\text{O}$ values range from ~3.2 ‰ to ~4.5 ‰ for the benthics (*C. teretis*) and from ~2.4 ‰ to ~3.6 ‰ for the planktics, with a mean $\delta^{18}\text{O}$ value of 4.03 ‰ (benthics) and 2.96 ‰, respectively. The prominent global shift in benthic $\delta^{13}\text{C}$ records during the late Miocene (>6.2 Ma) (Zachos et al. 2001) has not been recorded in Hole 910C (Fig. 3.3.2) confirming the age of the base to be younger than 6.2 Ma. Glacial stages/stadials are reflected in the $\delta^{18}\text{O}$ isotopic record as heavy excursion of variable amplitude, duration, and regional extent (Figs. 3.3.1). Amplitudes in the benthic $\delta^{18}\text{O}$ record can reach >1.5‰, but usually are between 0.3–0.8 ‰ and always correspond to low $\delta^{13}\text{C}$ values (< -1.0 ‰) indicating the influence of low-salinity, melt- or freshwater injections. However, two prominent low $\delta^{13}\text{C}$ values (< -3.0 ‰) correspond to rather heavy $\delta^{18}\text{O}$ values (> 4.0 ‰) (see “Highlight” discussion further below). Well-constrained glacial events during the late Miocene (TG20 at ~5.75; Si4 at ~4.85) (cf. Hodell et al. 2001) and late Pliocene (M2 glaciation at ~3.29 Ma, MIS 100, ~2.71-2.75 Ma) (Lisiecki and Raymo 2005) are clearly identified (Fig. 3.3.3) and used as 2nd order age fixpoints for the revised chronostratigraphy (see below). Fine tuning of the chronostratigraphy by correlating the early Pliocene $\delta^{18}\text{O}$ record of Hole 910C with the global LR04 stack (Lisiecki and Raymo 2005) reveal additional 12 fixpoints (see Table 1.1). The sedimentation rate model before and after tuning remains consistent (Fig. 3.3.4). A linear trend of rather moderate values (8-12 cm/kyr) occurs prior to 2.7 Ma. Post 2.7 Ma sedimentation rates are more variable with highs and lows ranging between 5 and >20 cm/kyr.

Modification of the isotopic record due to changes in bottom water temperatures may be excluded. Bottom water temperature reconstruction inferred from Mg/Ca analyses of benthic foraminifera (*Melonis barleanum*) remains rather constant (~1-3 °C), which considering the error margin of the applied calibration method (Kristjánsson et al. 2007) are only slightly warmer than modern observations (0 °C). Amplitudes of 0.5-1.0 ‰ between the Holocene mean value of *C. teretis* (3.8 ‰) and Miocene lows may reflect changes in the global ice volume, which would support our attempt to correlate the Miocene/early Pliocene $\delta^{18}\text{O}$ record with global glacial events (Zachos et al. 2001).

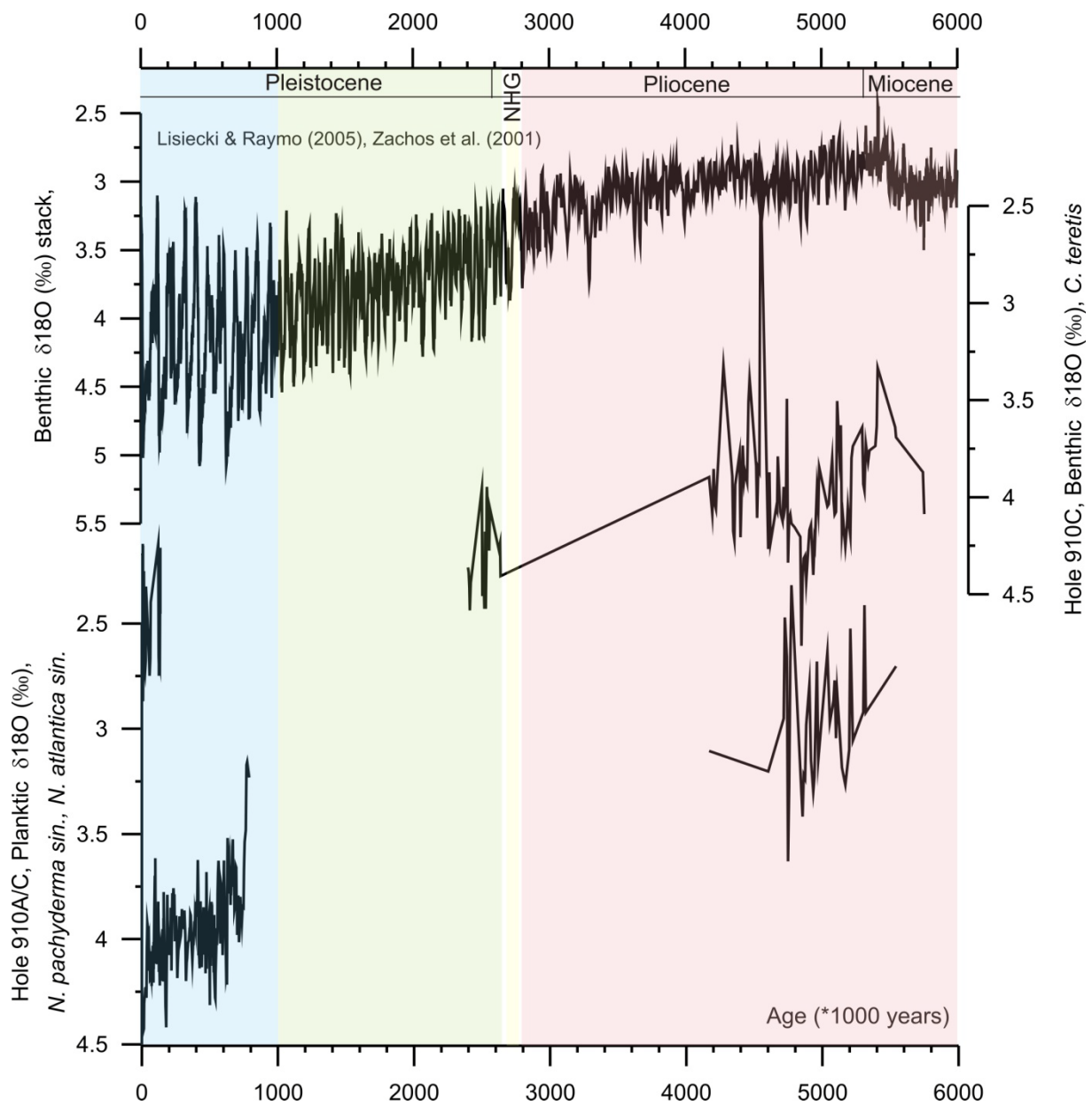


Fig. 3.3.1 Compilation of available benthic and planktic oxygen isotope data for Site 910 compared to the LR04 stack of Lisiecki and Raymo (2005). Data between ~5.8 and ~2.4 Ma are based on analyses of Hole 910C. Data from the last ~1 Ma have been published by Knies et al. (2007).

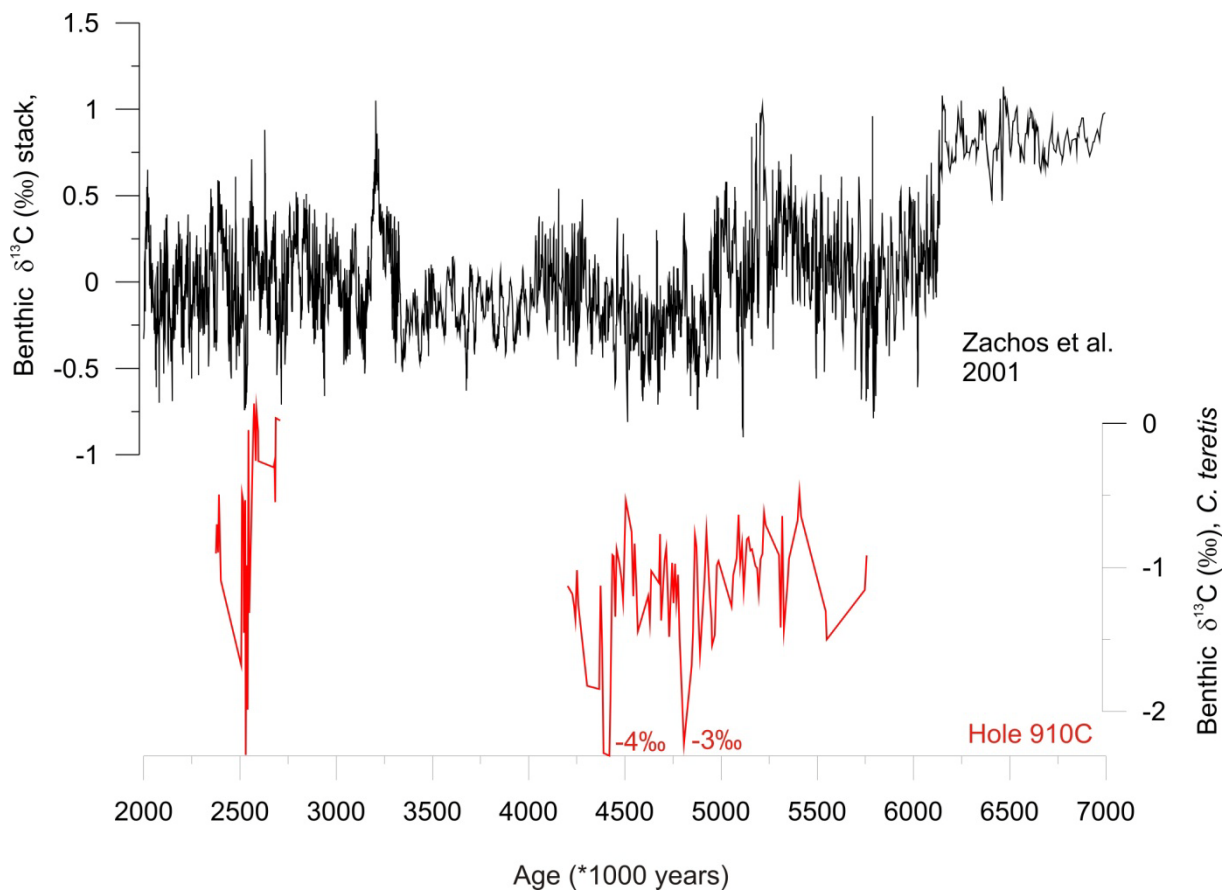


Fig. 3.3.2 Compilation of available benthic carbon isotope data ($\delta^{13}\text{C}$) for Hole 910C compared to global stack of Zachos et al. (2001). Note that we do not record the prominent $\delta^{13}\text{C}$ isotope shift to heavier values around 6.2 Ma.

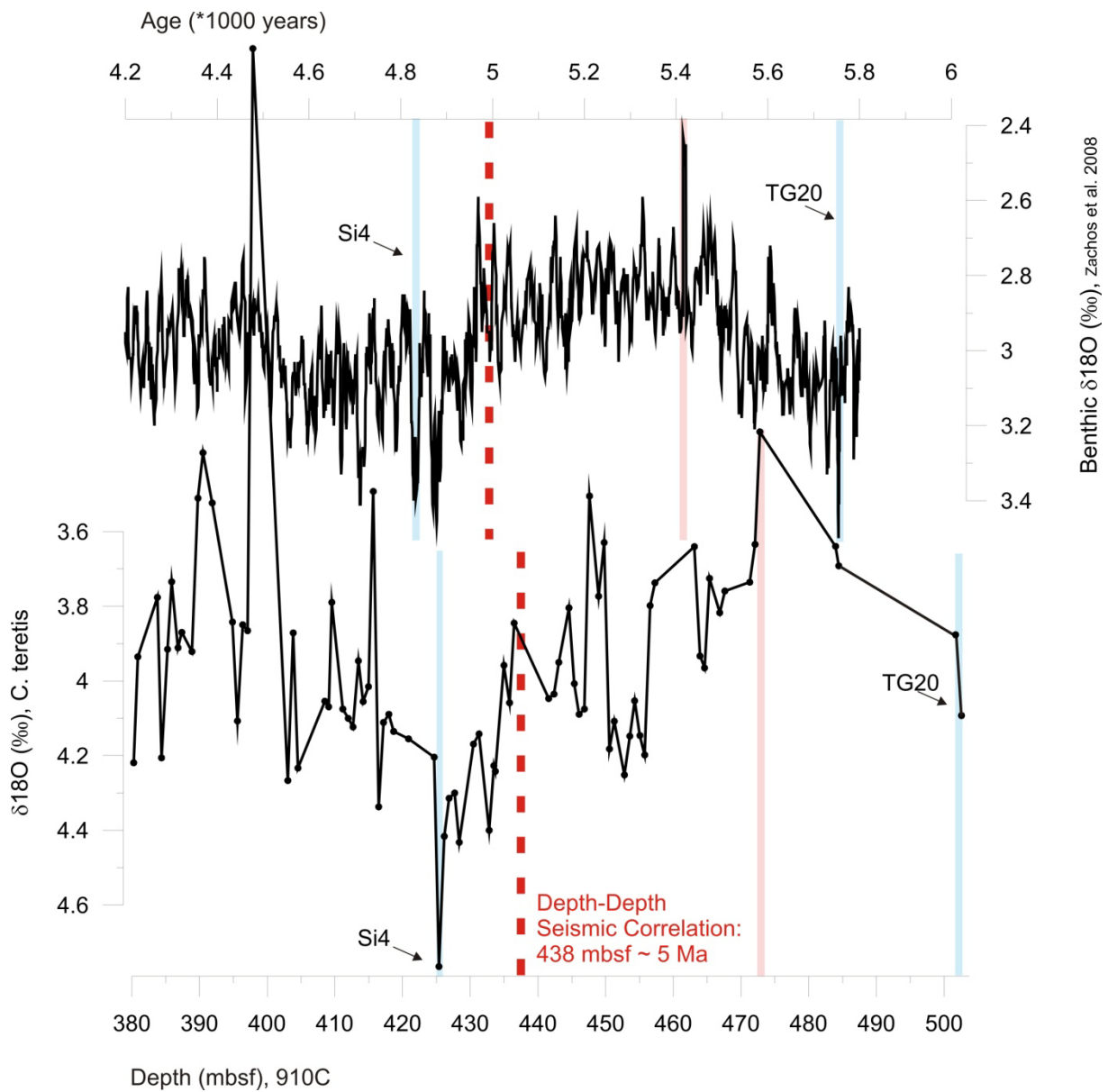


Fig. 3.3.3 Definition of additional tie-points by comparing stable oxygen isotope data of Hole 910C and Zachos et al. (2001) data set. Red stippled line indicates the correlation of the seismic reflectors between Hole 911A and 910C at 5 Ma. Light blue lines indicate glacial events Si4 and TG20 (Hodell et al. 2001). Light red line marks the correlation between light oxygen isotope values at ~5.4 Ma.

Sedimentation rates (cm/kyr), Hole 910C

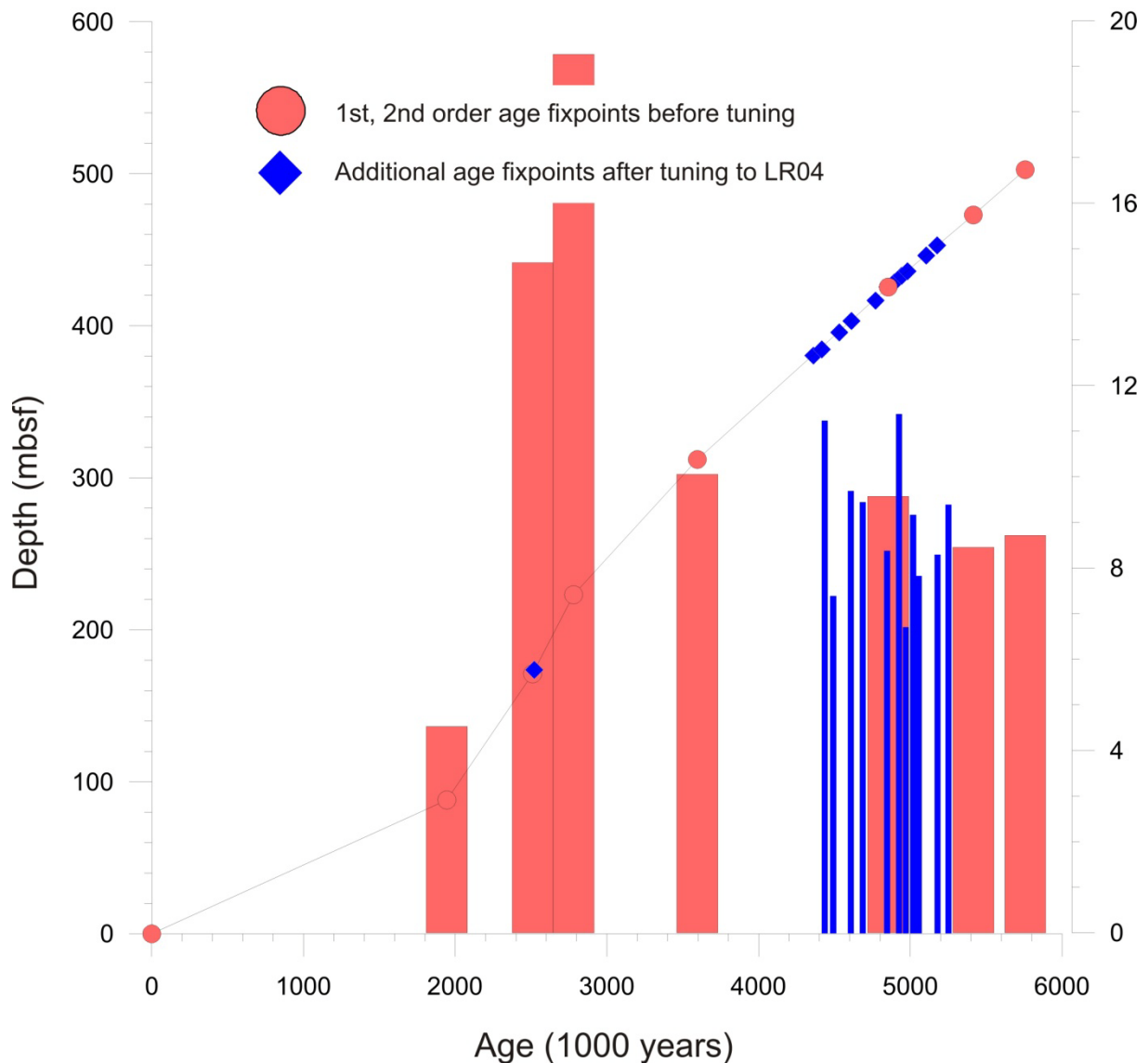


Fig. 3.3.4 Sedimentation rate model for Hole 910C

3.4 Module 2: Paleomagnetic record of Hole 910C and 911A (Karl Fabian, Geological Survey of Norway)

Interpretation of paleomagnetic signals in Hole 911A and 910C

The revised paleomagnetic records of ODP910C and ODP911A provide essentially new information for the construction of a comprehensive age model for the Yermak plateau. About 900 samples were investigated during course of the project.

Paleomagnetic records rely on a relatively continuous sediment accumulation with no or few hiatus and a syndepositional acquisition of remanent magnetization. Both prerequisites are not evident in the two cores and a detailed combined study of both rock magnetic and paleomagnetic records is required to infer chronostratigraphic information. The main

obstacles which complicate a direct paleomagnetic interpretation are the occurrence of greigite as a remanence carrier and a possible drilling overprint known to be present in older ODP drill cores. The strategy to overcome these disturbances is to use a stratigraphic alignment of both paleomagnetic records, which is achieved by following seismic reflectors across a high resolution seismic profile connecting the drilling sites of ODP910C and ODP911A (Figure 1.1). It is thereby possible to differentiate between coherent magnetic reversals indicating syndepositional remanence, and incoherent remanent magnetizations which then can be linked to late diagenetic greigite remagnetization, possibly due to gas or fluid flow (see Highlight chapter below). Using this approach, the paleo- and rock magnetic information even provides additional data to detect and characterize these fluid flow events. The basic mechanisms of synsedimentary and postsedimentary greigite formation are explained in Fig. 3.4.1. The smoothing effect of synsedimentary remanence acquisition is modeled in Fig. 3.4.2 which underlies the chronostratigraphic interpretation in the following paragraphs.

The paleomagnetic record of Hole 911A

Paleomagnetic sample cubes from undisturbed parts of Hole 911A below 342 m provide new inclination measurements that coincide well with the whole-core shipboard measurements in the overlapping depth interval down to 400 m (Fig. 3.4.3). The Matuyama-Gauss boundary, which was reported in this interval by the initial report (Flood et al. 1995), is also found in the resampled data set at about the same position. In contrast to the shipboard data, the new sample set also shows a distinct reversal sequence in the lower sediment section down to 505 m (Fig. 3.4.3). Because of the decreased accumulation rate below 400 m and the delayed syndepositional remanence acquisition (Fig. 3.4.2) it is not straightforward to correlate this sequence to the GPTS. Depth dependent smoothing effects due to delayed remanence acquisition, as modeled in Fig. 3.4.2, can encompass much larger time intervals Δt when sediment accumulation is low. Yet, the observed inclination sequence provides several important pieces of information. First it excludes that large scale remagnetization dominates the magnetic signal, otherwise a uniform inclination from the remagnetization event would prevail (Fig. 3.4.1e). Second, the spacing of the clearly distinguishable reversals substantially constrains the possible temporal interpretation, and third, in combination with biostratigraphic indications, clear reversal boundaries can serve as tie points for the time scale, although the shift due to the delayed syndepositional remanence acquisition must be taken into account. All inferred reversal boundaries for Hole 911A are summarized in Table 1.1. We suggest that the base of Hole 911A encompasses sediments deposited during the Thvera subchron (~5.0 – 5.3 Ma).

Correlation of paleomagnetic records of Hole 911A and Hole 910C

The seismic correlation between Hole 911A and 910c provided the unique opportunity to compare the two paleomagnetic records based on the assumption that synsedimentary remanence acquisition should lead to closely related inclination variations in both sequences. This required to obtain a detailed paleomagnetic record of Hole 910C, which also was of interest, because 910C appeared to have much higher sediment accumulation rates in the lower parts of the sequence in comparison to Hole 911a.

Therefore, the magnetic remanence of each of 491 samples, covering the depth interval from 151.35 m to 504.35 m in Hole 910C, was measured and characterized. Using the seismic correlation and the proposed age model, the data of Hole 910C are plotted in Fig. 3.4.4 versus the inclination data from Hole 911A. The result clearly confirms the interpretation of the NRM sequence in ODP 911A as synsedimentary remanence, because the upper parts of both

cores essentially show the same inclination signal. Differences in the position of inclination changes can easily be explained by minor offsets in the depth-depth correlation between the holes, or by differences in the delay time for syndepositional remanence acquisition. The second important information from the paleomagnetic record of Hole 910C is that it clearly shows a remagnetization event below ~ 4.2 Ma where the signals from the two holes start to deviate significantly, and Hole 910C continuously displays a positive inclination down to the bottom. This signal implies several important facts. First, it indicates the presence of fluid flow activities around 4 Ma at the Yermak plateau. Second, it confirms that these fluid flow events are localized and probably focused along fault lines. Third, it supports the remagnetization model in in Fig. 3.4.1 e, and fourth, it indirectly also supports the syndepositional remanence interpretation of Hole 911A.

To summarize, the combined paleomagnetic records of Hole 911A and Hole 910C provide clear evidence for a syndepositional remanence acquisition in Hole 911A and in Hole 910C down to about 4.2 Ma. Stratigraphic tie points (Table 1.1) from polarity reversals have an uncertainty due to delayed remanence acquisition, but can be used in combination with biostratigraphy to constrain the sedimentation history. A uniform overprint in Hole 910C below about 4.2 Ma indicates a major localized fluid flow event.

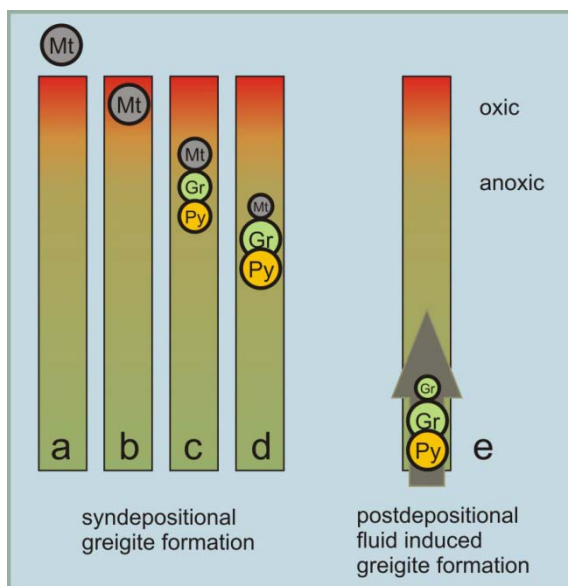


Fig. 3.4.1 Simplified sketch of syndepositional and postdepositional greigite formation modified from Oda and Torii (2004). After deposition of magnetite (a), magnetic remanence in the oxic sediment zone aligns with the external magnetic field (b). Further sediment accumulation brings the magnetite in the anoxic zone where additional authigenic greigite and pyrite are formed (c). Here the greigite acquires a syndepositional remanent magnetization (c-d) which reflects the external field at some delay time Dt after deposition ($Dt \sim 10-50$ ka). In contrast, a later fluid flow event partly or fully remagnetizes the sediment by uniformly overprinting the whole sediment sequence with a later field direction (e). The absence of such a large-scale uniform overprint therefore indicates syndepositional remanence acquisition.

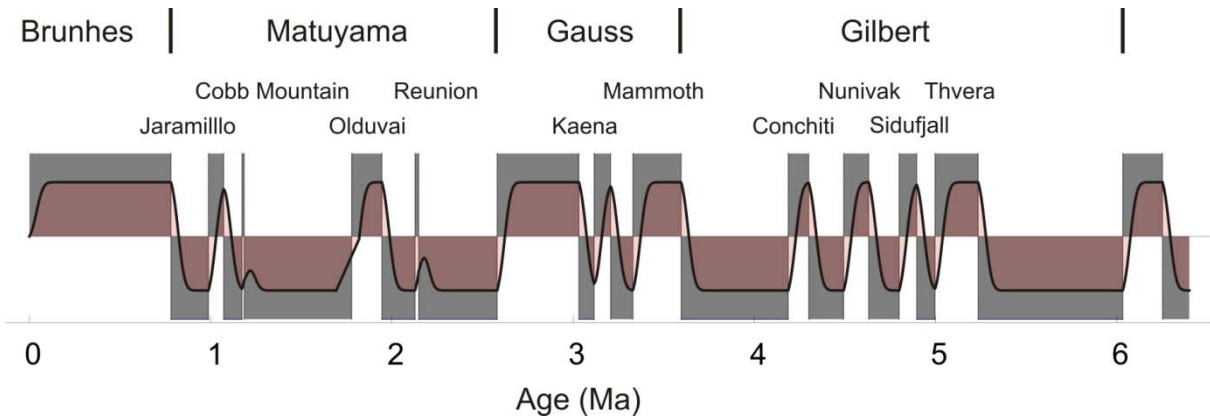


Fig. 3.4.2 Polarity chrons and subchrons of the GPTS for the last 6-Ma. The plot shows the ideal inclination record where normal fields have positive, and reverse fields negative inclinations. The red line shows the effect of a smooth syndepositional remanence acquisition with an average delay of 50 ka. Note that short subchrons like the Cobb Mountain or Reunion are completely smoothed out, while others appear considerably shorter and may be lost at low sampling density.

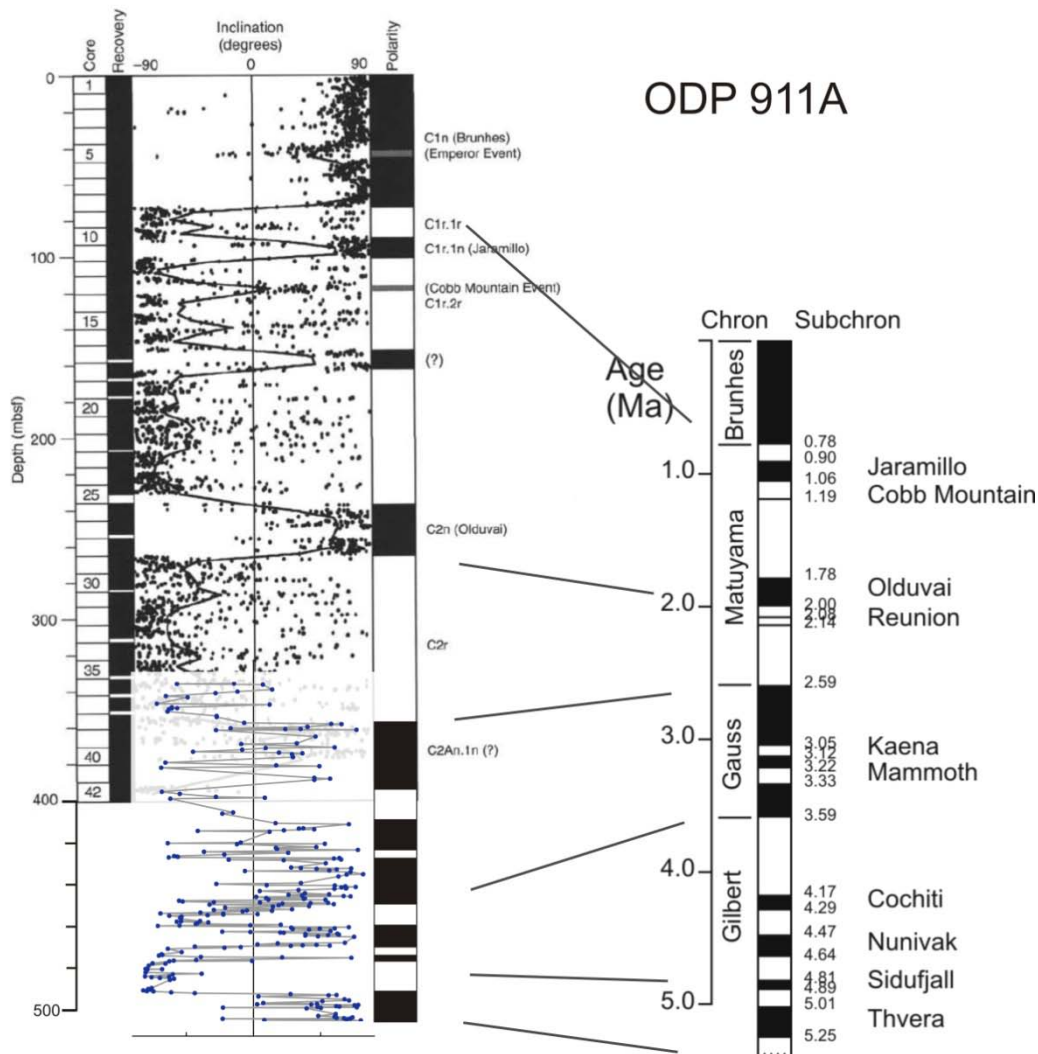


Fig. 3.4.3 Inclination of the natural remanent magnetization of ODP911A versus depth. The graphics combines the shipboard results from the initial report (Flood et al., 1995) and automatically determined inclination values of the new measurements (blue). Note the good fit in the overlapping region, and the substantially lower accumulation rate in the deeper part of the core. The latter agrees with the seismic data.

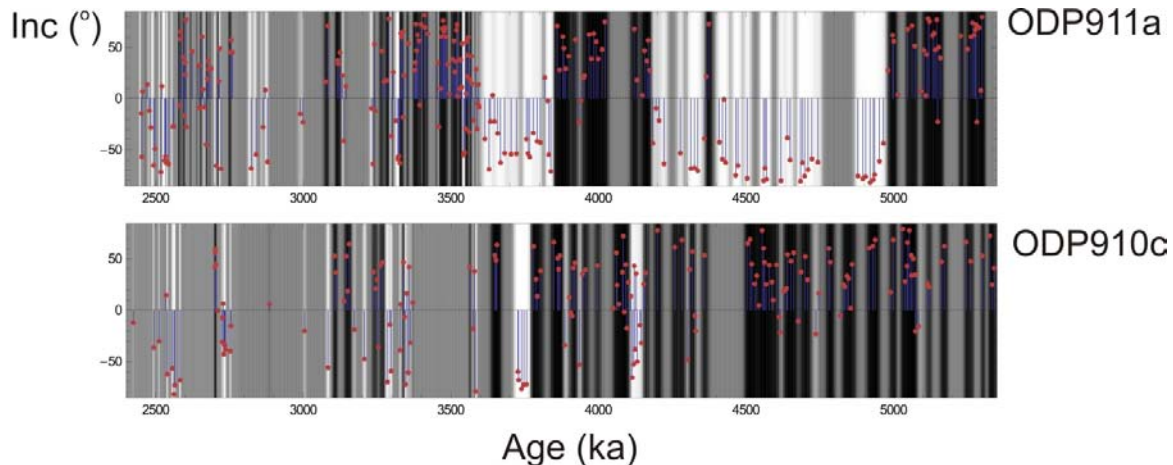


Fig. 3.4.4 Comparison of the paleomagnetic inclination data from Holes 910C and 911A. Using seismic correlation together with the suggested age model, both data sets are plotted on a common approximative age scale. Down to about 4.2 Ma both records have large similarities and can be interpreted as reflecting two syndepositional records of the same geomagnetic field but with different delays in remanence acquisition, and possibly minor partial overprints. Below 4.2 Ma Hole 910C apparently reflects a postdepositional complete overprint, whilst Hole 911A continues to show the geomagnetic field variation.

3.5 Module 3: Seismo-stratigraphic framework of the western Svalbard/Barents Sea margin (PI: Karin Andreassen, University of Tromsø)

Seismic Database

The University of Tromsø (UiT) has compiled an extensive digital seismic database for the Western Svalbard - Barents Sea area (Fig. 3.5.1). Most of the compiled data consist of multi-channel seismic from the industry and the Norwegian Petroleum Directorate. Some high-resolution lines had been acquired by the University of Bergen, the Norwegian Polar Institute and MAGE (Murmannsk Arctic Geological Expedition). The main objective of establishing a seismic-stratigraphic framework for the ODP wells at the Yermak Plateau and correlation southwards to ODP well 986 required acquisition of new, seismic data to improve resolution and to allow correlation. During this project 1 700 km of high-resolution single-channel seismic data was therefore acquired from the western Svalbard Margin during three scientific cruises with the research vessel of UiT (Fig. 3.5.1).

The new seismic data include for the first time a high-resolution seismic transect across the Yermak Plateau crossing all three ODP sites on the plateau (Fig. 3.5.1). The acquisition of this line, in an area that is usually ice-covered most of the year, was made possible due to favorable ice conditions in the fall of 2010.

Seismic correlation

The established age fix-points from ODP sites 910 and 911 (Tab. 1.1) have been converted from meters below seafloor to two-way travel-time using equations from the ODP Initial Report (Myhre et al., 1995), and have been assigned respective seismic horizons. The new age model for sites 910 on the crest and 911 on the eastern slope of the Yermak Plateau correlate well on the seismic data (Fig. 3.5.2). The seismic correlation of the age fix-points from the two sites are quite straight-forward for fix-points younger than ~2 Ma, as the stratigraphy has a mostly continuous and parallel reflection configuration with few faults. These age fix-points are also easy to extend westwards towards site 912 on the western slope. Due to erosion of the

Yermak Plateau crest, none of the age fix-points from ODP site 911 younger than ~2 Ma can be correlated directly towards ODP sites 910 and 912 (Fig. 3.5.2). Based on the available seismic grid the erosion is persistent on the whole Yermak Plateau and it has not been possible to bypass. Due to this, the existing age model for ODP site 912 (Myhre et al., 1995) has been used for reflections younger than 2 Ma on the western side of the Yermak Plateau. This age model has been time-converted using velocity information from the Initial Report (Myhre et al., 1995). Since site 912 only penetrates to an age between 2 and 2.5 Ma, the only horizon which can be correlated directly from 911 in the east through 910 on the crest towards 912 in the west is the horizon corresponding to the age fix-point of 1.95 Ma. Most of the seismic horizons, except those affected by erosion on the crest of the Yermak Plateau can be traced as continuous reflections on the seismic grid on the southern Yermak plateau and on the slope outside northwest Svalbard.

Three key seismic horizons have been selected and are correlated southwards towards ODP site 986 on the Western Svalbard margin 300 km south of ODP site 912 (Fig. 3.5.3, Figure 2.1):

(1) a horizon of 0.78 Ma, which corresponds to the age of reflector R3 in the southwestern Barents Sea (Faleide et al., 1996).

(2) a horizon of ~2.7 Ma, which represents the beginning of the Pleistocene and which corresponds to the age of reflector R7 (Knies et al. 2009);

(3) a reflector which marks a significant event with the beginning of deep drafted icebergs on both the eastern and western slopes of the Yermak Plateau, which based on correlations to site 911 and 912 have been assigned an age of ~1.5 Ma, which corresponds to the age of reflector R5 (Faleide et al., 1996).

The 0.78 Ma and 1.5 Ma seismic reflectors can be traced all along the margin from site 912 to site 986, but the 2.7 Ma horizon can only be traced south from site 912 to the Isfjorden Trough Mouth Fan (Fig. 3.5.3). The available seismic line from site 986 northwards is a high-resolution single channel line without enough penetration to image the 2.7 Ma horizon below the Isfjorden Trough Mouth Fan.

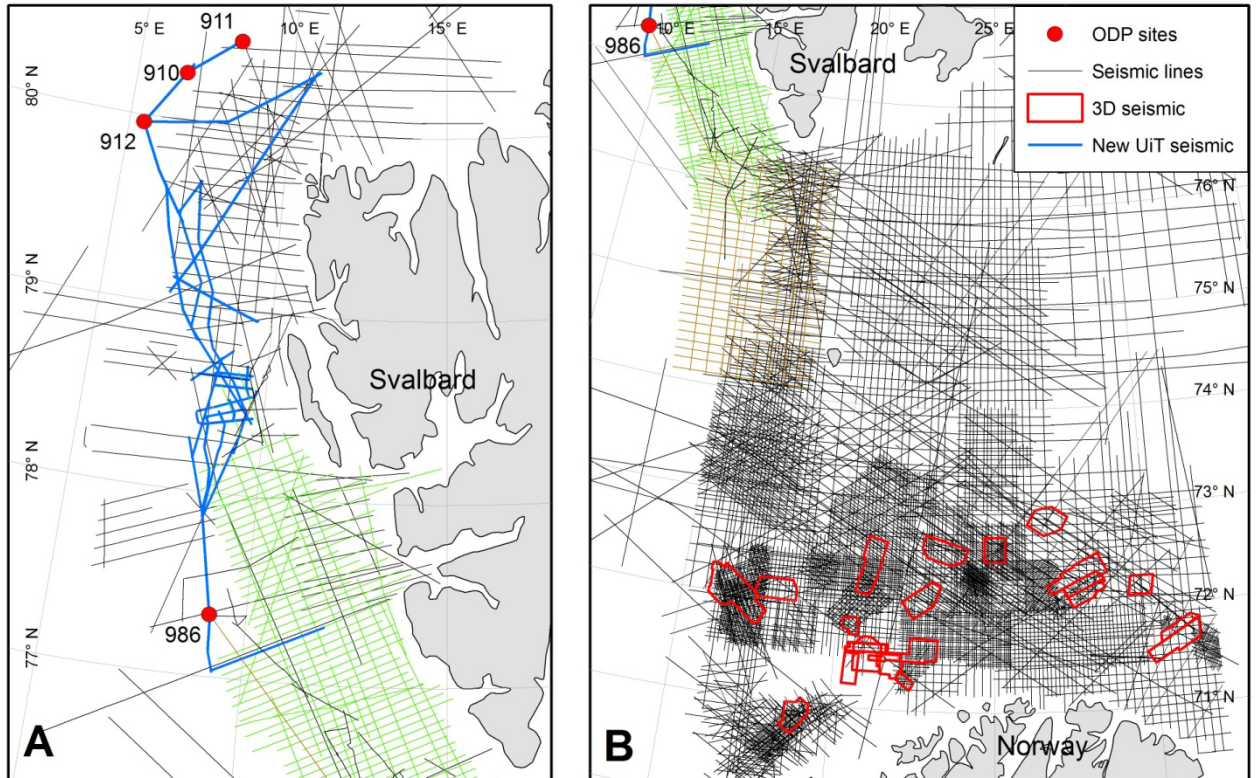


Fig. 3.5.1: Maps revealing the available seismic data (database at UiT). The green and light brown lines are from MAGE, only the brown have been available for this study, (A) Western Svalbard margin. (B) Western Barents Sea.

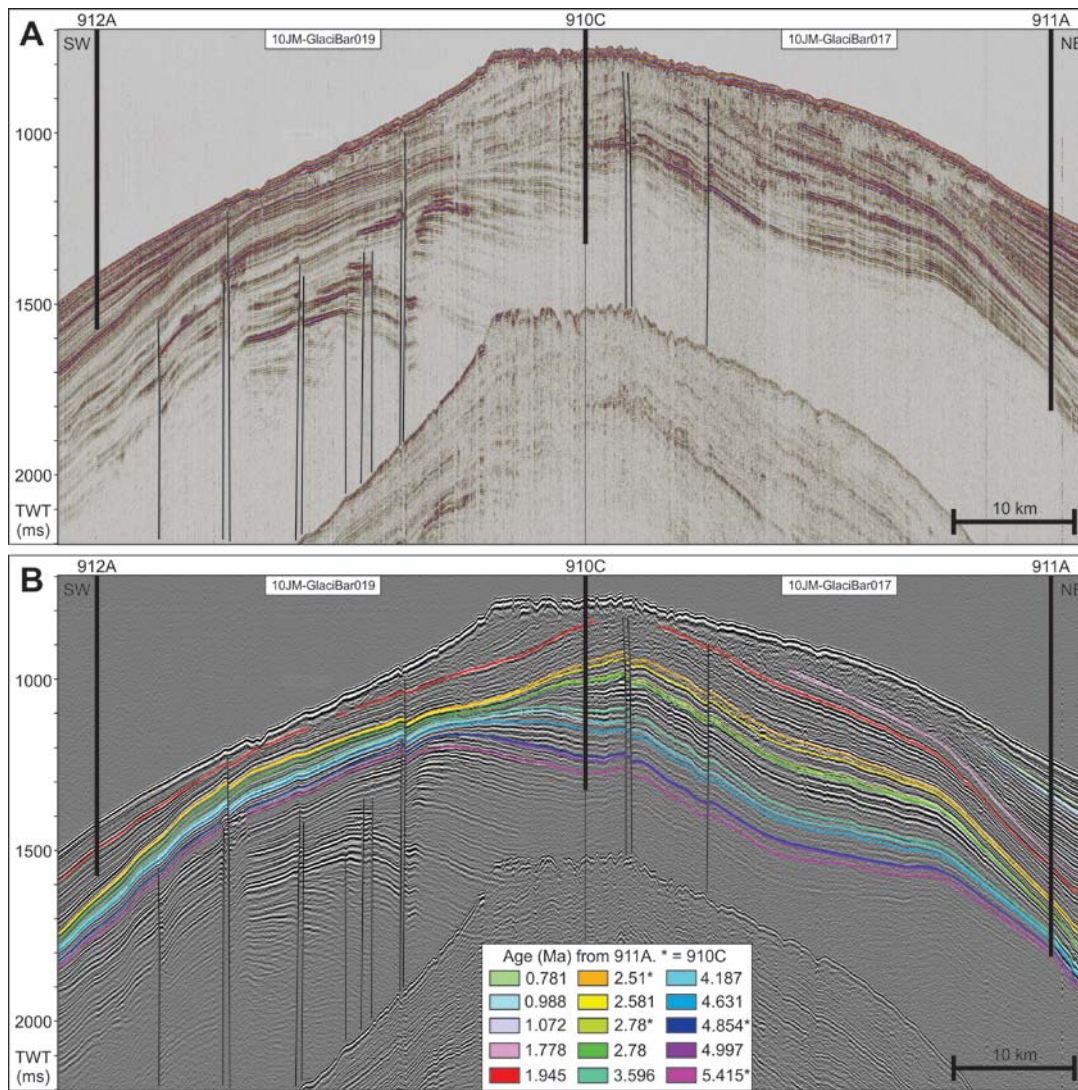


Fig. 3.5.2 (A) High-resolution seismic transect across the Yermak Plateau crossing ODP sites 912, 910 and 911. (B) Same as A, but with interpreted horizons based on age fix-points from the studied ODP holes 911A and 910C.

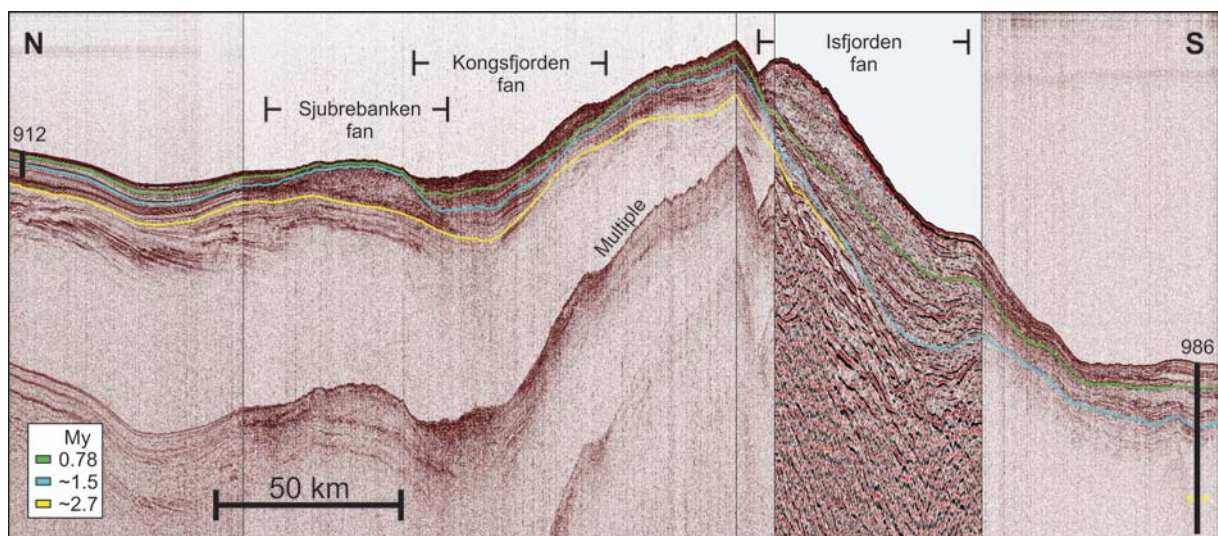


Fig. 3.5.3 Composite seismic transect from ODP site 912 west of the Yermak Plateau southwards to ODP site 986 on the western Svalbard margin. Location of trough mouth fans is indicated.

4. A NEW CONSISTENT AGE MODEL FOR THE YERMAK PLATEAU

The main objective of the project is namely to establish a new chronostratigraphic framework of ODP Site 911 and 910 is successfully achieved. Firstly, the seismic correlation between both sites shows that the base of Hole 910C is significantly older than the base of Hole 911A (Figure 1.1). From 1st order age fixpoints derived from biostratigraphic and paleomagnetic data we infer the recovery of late Miocene/early Pliocene sediment sequences in both holes (Tab. 1.1). From 2nd order age fixpoints (Tab. 1.1) derived from correlating global stacks of oxygen isotope data (Zachos et al. 2001, Lisiecki & Raymo 2005) with new benthic oxygen isotope data of Hole 910C (Fig. 3.3.3) we further propose that the base of Hole 910C is ~5.8 Ma old. We argue that the tie point at 438 mbsf (4.997 Ma) inferred from seismic correlation between Hole 910C and 911A marks the boundary between two intervals characterized by heavier (~4.9-4.6 Ma) and lighter $\delta^{18}\text{O}$ values (~5.5 – 5 Ma) (Zachos et al. 2001, Lisiecki & Raymo 2005). The marine isotope stage event Si4 (~4.85 Ma) has been identified at 425 mbsf (Fig. 3.3.3). Few data points at the base of Hole 910C, however, makes the definition of further tie-points problematic. By linearly extrapolating the sedimentation rate from the latest tie-point (Si4: ~4.85 Ma) towards the base of Hole 910C, we achieve a base age of ~5.7 Ma. Hence, we suggest that the heavy $\delta^{18}\text{O}$ value at 502.6 m correspond to the marine isotope stage event TG20 at ~5.75 Ma (Hodell et al. 2001). The base of Hole 910C is tentatively dated to be ~5.81 Ma.

A number of 1st order age fixpoints have established a robust chronostratigraphic framework for Hole 911A (Tab. 1.1). The lowermost tie-point is defined at ~492 mbsf dated to be 4.997 Ma (Top Thvera subchron). The base age of Hole 911A, however, is still somewhat uncertain and tentatively placed around the Pliocene/Miocene boundary (see chapter 3.1/3.2 for more details). A base age of ~5.3 Ma in Hole 911A is further inferred by correlating sedimentological/geochemical data between both holes upon our 1st and 2nd order age models. We used titanium (Ti) concentrations (in mg/kg) in the sediments as proxy for terrigenous material either supplied by glacial or glacio-fluvial processes of Proterozoic sediments from western and northern Svalbard (Ottesen et al. 2010). The Ti records for Hole 911A and 910C are nearly identical for the lower part of the boreholes (Fig 4.1) suggesting that the material was deposited contemporaneous. In contrast to previous reports (Myhre et al. 1995), indications of a hiatus at the bottom of Hole 911A have not been found. Instead, a condensed section with significantly lower sedimentation rates (~3-6 cm/ka) compared to the late Pliocene (~15-20 cm/ka) is proposed (Fig. 3.3.4). The new age models for Hole 911A and 910C based on all available biostratigraphic and paleomagnetic data are summarized in Figure 4.2

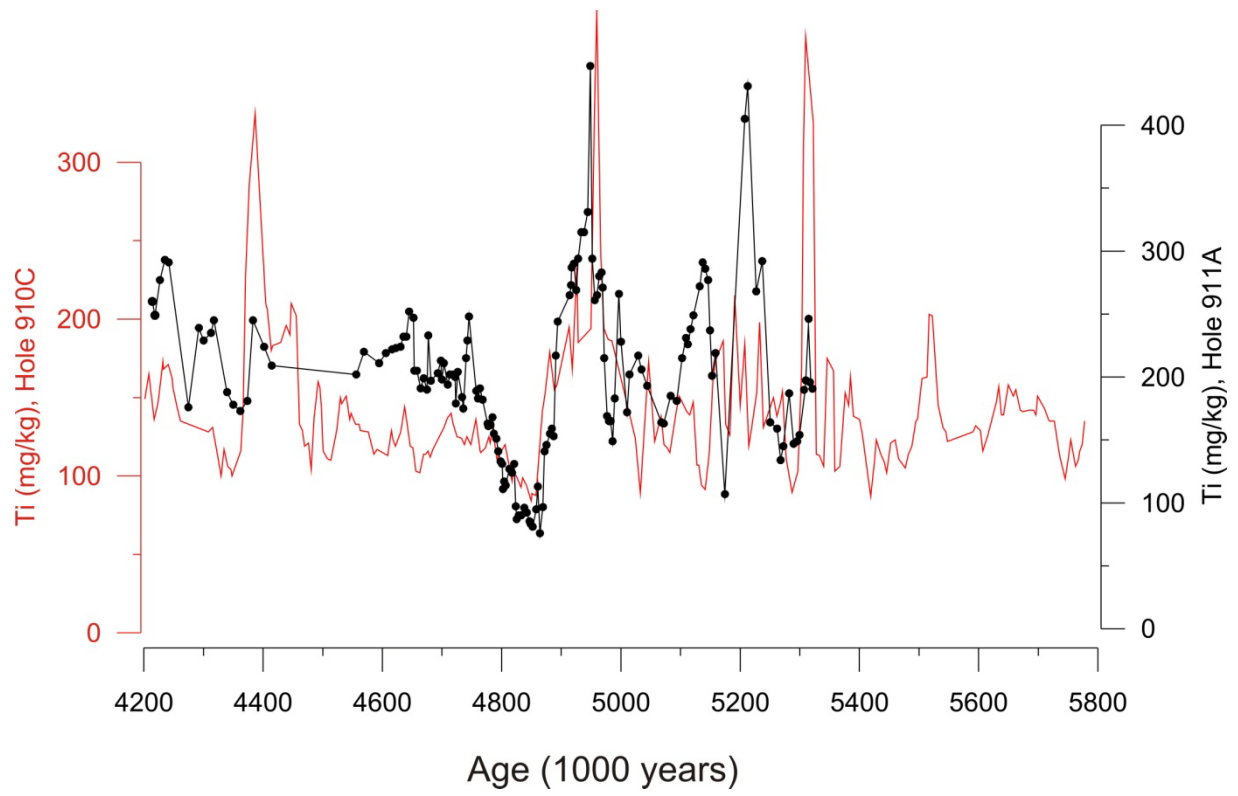


Figure 4.1 Titanium content (mg/kg) in sediments deposited between 4.2 and 5.8 Ma in Hole 911A and 910C.

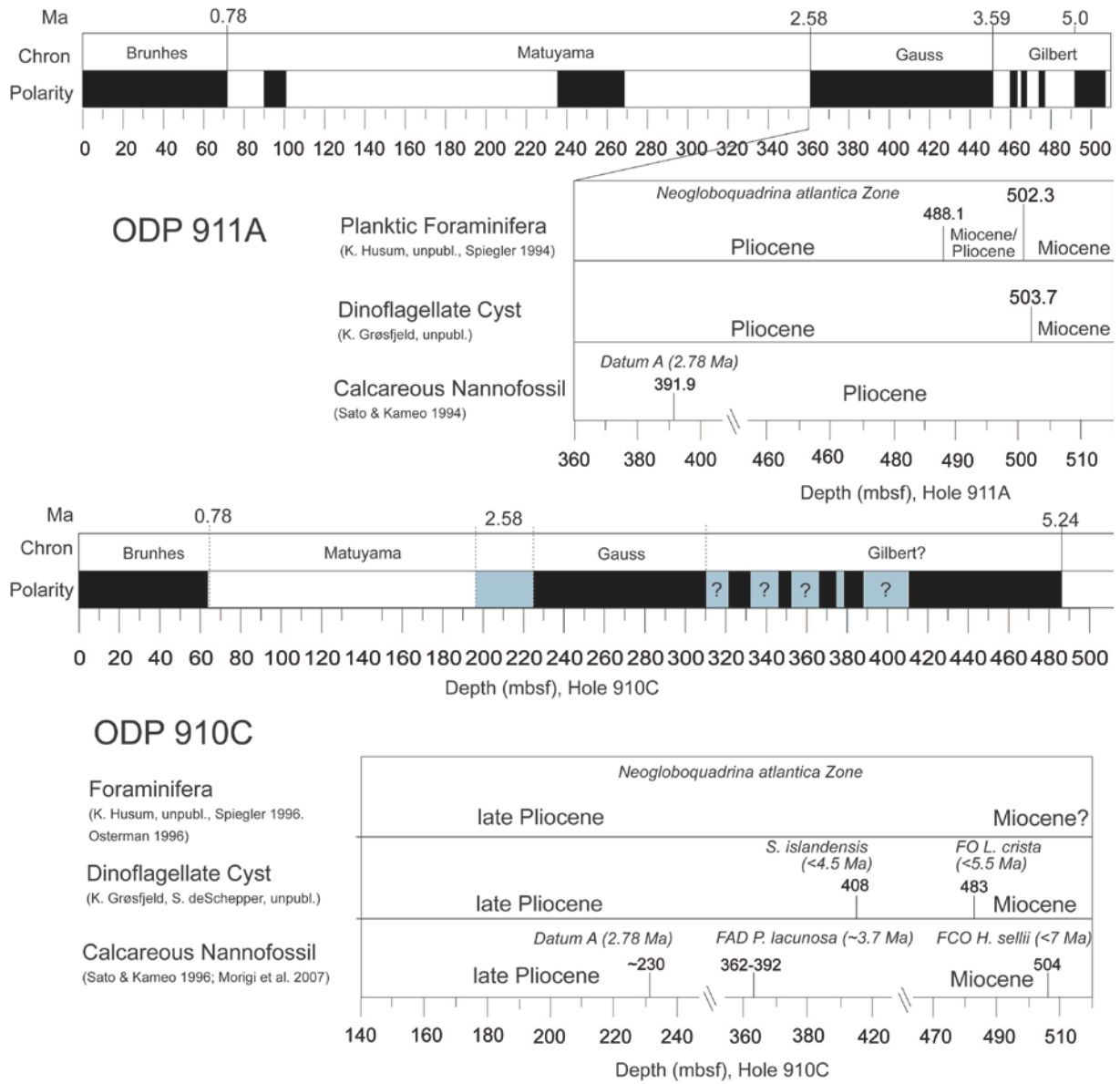


Figure 4.2 Compilation of chronostratigraphic data for Hole 911A (A) and Hole 910C (B)

5. PALEOCLIMATIC IMPLICATIONS

In addition to our main objective improving the chronostratigraphy of the Yermak Plateau, the new age model and borehole data provide the opportunity to discuss paleoceanographic and -climatic constraints in the Atlantic-Arctic gateway. This work is currently in progress.

Available data will be further analysed during course of the Petromaks “GlaciBar” project. Nevertheless, major findings have been compiled and will be presented below:

Highlights Module 1: Planktic and benthic foraminifera

The benthic foraminiferal assemblage in Hole 910C consists of subarctic – arctic species. *Cassidulina reniforme* and *Elphidium excavatum* increase upwards and are showing an overall cooling through the Pliocene (Fig. 3.1.1). *Islandiella helenae/norcrossi* depend on nutritious water masses and are often found near the sea ice boundary (e.g. Hald and Steinsund, 1996) and associated with high organic carbon flux (Jennings et al. 2004). Two maximum intervals of this group during the early Pliocene could reflect a closer position of the sea ice boundary. Enhanced supply of fine sands and organic debris (see Figure 5.2) may support this interpretation. The species *Cassidulina teretis*, an indicator of chilled Atlantic water (Mackensen and Hald, 1988), show a general continuous inflow of Atlantic water to the study area through the Pliocene. *Epistominella vitrea* and *Melonis barleanus* are both associated with food availability. *E. vitrea* is an opportunistic species that react quickly to high food availability (Jorissen et al, 1992), whereas *M. barleanus* prefer partially degraded organic matter (Korsun and Polyak, 1989). Due to the poor preservation of the planktic specimens only a qualitative analysis was performed on the planktic foraminifera. The planktic foraminiferal assemblage in Hole 910C comprises the modern species *Neogloboquadrina pachyderma* (sin). This species dominates modern subpolar – polar environments and is quite temperature depended (Be and Tolderlund, 1971). The other modern species *Neogloboquadrina pachyderma* (dex) and *Globigerina bulloides* are characteristic of warmer sea surface temperatures than *Neogloboquadrina pachyderma* (sin) (e.g. Be and Tolderlund, 1971). The fluctuations of *G. bulloides* could imply intervals of higher sea surface temperatures during the Mid Pliocene. However, the preservation of the planktic species is very poor, hence this occurrence in Mid Pliocene may just reflect better preservation during this time interval rather than oceanographic fluctuations. Analysis of the foraminiferal assemblages of Hole 911A show both benthic and planktic foraminifera (Fig. 3.1.2). The results suggest that the benthic foraminiferal assemblages are not reworked and belong to a subpolar – polar environment. However, the preservation is too poor to perform a quantitative analysis, and only the planktic fauna was quantitatively analyzed showing an Arctic assemblage. The fauna is dominated by *N. atlantica* (sin), and sporadic occurrences of the modern species *N. pachyderma* (sin) reflect the high latitude conditions (e.g. Be and Tolderlund, 1971).

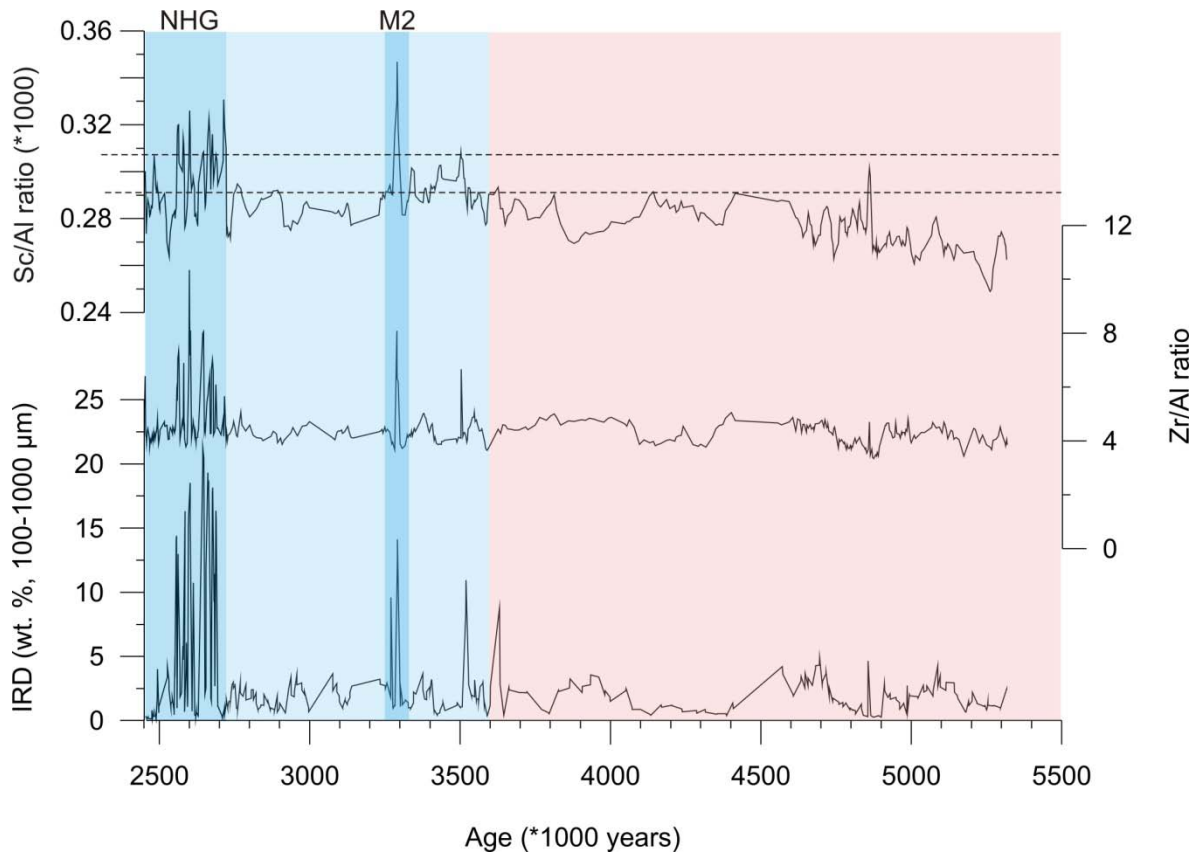


Figure 5.1 Compilation of IRD (>100 μm %), Zr/Al and Sc/Al ratios vs. age in Hole 911A. Distinct IRD events are marked in blue. Red interval shows the period with very limited or no IRD in Hole 911A

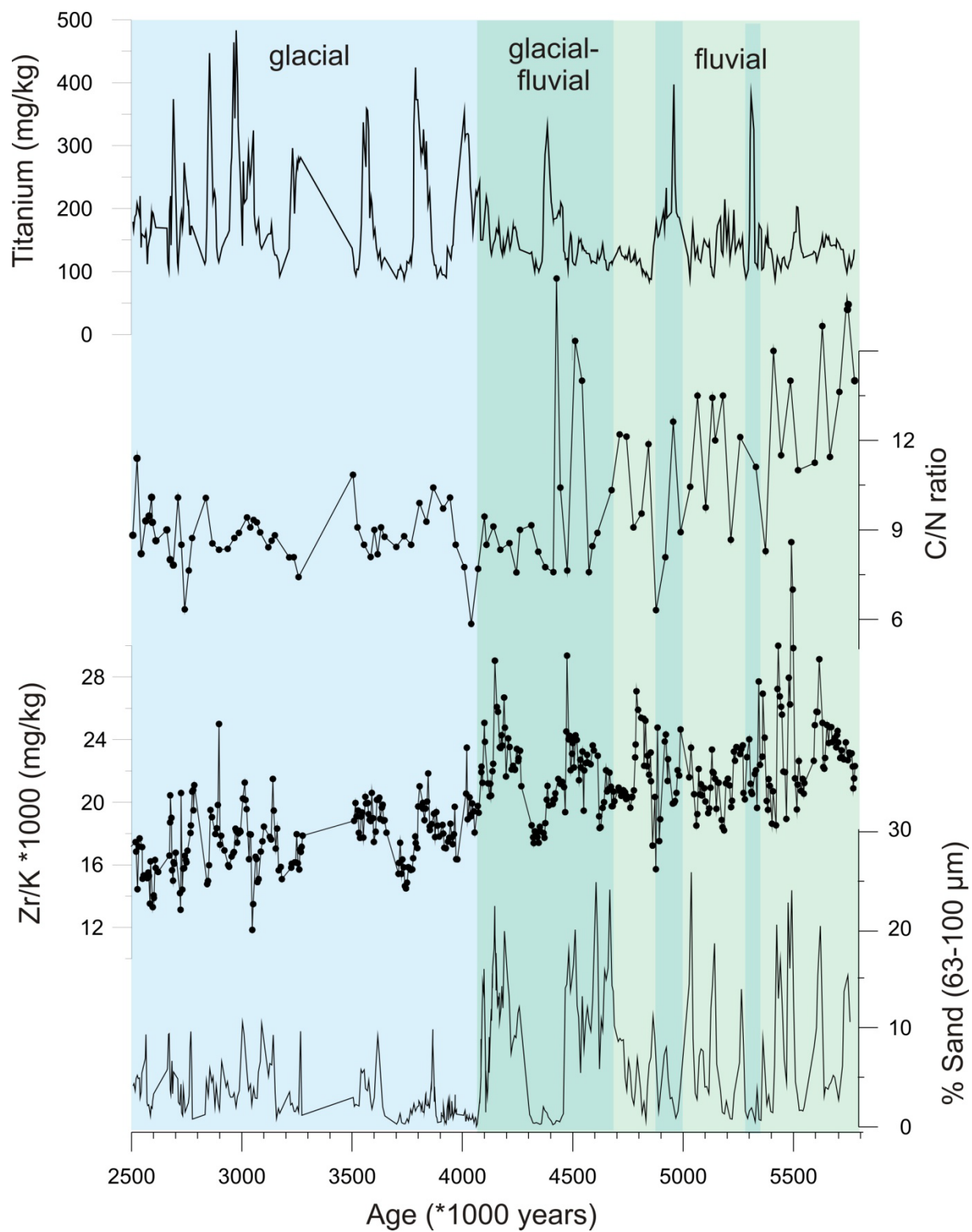


Figure 5.2 Compilation of fine sand content (% 63-100 μm), Zr/K ratio, C/N ratios, and titanium content in Hole 910C between 5.8 and 2.5 Ma.

Highlights Module 1: Ice rafted debris and glacial dynamics

The development of the Svalbard/Barents Sheet ice sheet during the late Pliocene/Pleistocene (post ~2.7 Ma) has been recently revised (Knies et al. 2009, Laberg et al. 2010, Laberg 2012) and additional inferences from the new seismo-stratigraphic framework is given further below (Highlights Module 3). Here, we focus on the pre ~2.7 Ma deposits providing new insights onto the abruptness of NHG and the transition from an exposed, vegetated Barents Sea during the late Miocene/early Pliocene to a fully glaciated Barents Sea at reflector R5 time (~1.5 Ma) (see below).

The IRD record (>100-1000 μm) of Hole 911A provides a regional view on the ice sheet extent in the northern Barents Sea beyond the coastline (probably towards the shelf edge). We have registered two major IRD events between ~5.3 and ~2.5 Ma: (1) during the “M2 glaciation”; the first major global glacial event during the initial NHG and (2) at ~2.7 Ma (Figure 5.1) where the ice protruded towards the northern and western shelf edge. IRD maxima corroborate with enhanced Zr/Al and Sc/Al ratios illustrating enhanced supply of glacially derived coarse-grained material from northern Svalbard; the nearest point source for both zirconium and scandium (Ottesen et al. 2010). The absence of IRD during major parts of the Miocene/Pliocene sequence excludes the presence of glacial ice near the coastline. In Hole 910C, a prominent increase in the number of dropstones at ~2.7 Ma (220 mbsf) mark the intensification of the NHG (Myhre et al. 1995). Prior to 2.7 Ma, we observe distinct input of fine sand (63-100 μm) associated with enhanced Zr/K ratios between 5.8 and 4.1 Ma (Figure 5.2). By normalizing Zr on K, an ubiquitous element in overbank sediments on Svalbard (Ottesen et al. 2010), we suggest the Devonian Old Redstone on northern Svalbard as the most likely source for the fine sand (Figure 5.2). The latter is associated with highest amount of pollen assemblages (Willard 1996, Schafstall 2011) and fresh organic plant materials (high C/N ratios) (Figure 5.2). Terrestrial palynoflora suggest the presence of boreal forest to subarctic tundra in the source area (Willard 1996, Schafstall 2011). The inferred proximity to the shoreline - and (glacial-) fluvial sediment transport to the shelf break – and dominantly current-influenced regimes on the Yermak Plateau suggest the sub-aerially exposed, vegetated Barents Sea region as the most likely source of the terrestrial organic-rich fine sands during the late Miocene – early Pliocene.

Short-term pulses of Ti-rich deposits, mainly concentrated in the fines, are observed during minor cooling phases during the early Pliocene (e.g. Si4) (Figure 5.2). Higher frequencies, however, occur between 4.0 – 2.5 Ma and corroborate with tectonic uplift and tilting along the margin and global climate deterioration (e.g. Stoker 2005a,b; Dahlgren et al. 2005; Ryseth et al. 2003). Ti-rich sediments are either originated from the Scandinavian mainland or – more likely – from Proterozoic deposits on western/northern Svalbard (Ottesen et al. 2010). Enrichments in the fines suggest the North Atlantic Drift as the main transport agent mainly through erosional processes (e.g. internal wave). Alternatively, cross-shelf transport either gravity-driven by conservative properties (temperature, salinity) or detachment of the bottom nepheloid layers is responsible for the sediment transport to the Yermak Plateau. Whether the Ti-rich sediment pulses follow climate patterns during the mid-late Pliocene is currently uncertain. However, we speculate that higher frequencies of Ti pulses since ~4 Ma is related to enhanced, glacially induced erosion on Svalbard and mark a gradual transition from densely vegetated to more glaciated landmasses on the exposed Barents Sea during the Pliocene. The distinct change at ~4 Ma corroborates with the early Pliocene unconformity observed along the NW European margin (Stoker et al. 2005a,b; Praeg et al. 2005). Uplift of

the NW Svalbard/Barents Sea region during the early-mid Pliocene may have changed routing of hinterland sediment supply and fostered the accumulation of glacial ice.

Highlights Module 2: Fluid flow inferred from greigite mineralization and stable isotopes

Greigite (Fe_3S_4) can form in association with microbially-mediated processes such as sulphate reduction, anaerobic oxidation of methane (AOM), and formation of gas hydrates (Roberts et al. 2011). In addition, the identification of greigite in ancient sediments may be useful to detect former gas hydrate systems (Larrasoana et al. 2007). At the sulfate-methane transition zone (SMT), released HS^- by bacterial sulfate reduction and AOM react with iron oxides resulting in formation of iron sulphides such as pyrite and/or greigite (Kasten et al. 1998). The formation of either pyrite or greigite depends largely on the availability of reactive iron (Kao et al. 2004); if reactive iron is abundant, limited amounts of hydrogen sulfide will react with iron and pyritisation reactions will not proceed to completion, thereby enabling preservation of greigite. In gas-charged sediments (e.g. Hydrate Ridge), favorable conditions for the formation of greigite are a limited source of sulphide and low concentration gradients of methane near disseminated gas hydrates (Larrasoana et al. 2007).

Preservation of greigite in Hole 910C occurred prior to 2.7 Ma as evident from susceptibility highs, and mineral inspection (Figure 5.3). In contrast, the sediment sequence deposited during the last 2.7 Ma does not show any evidence for the presence of greigite; however keeping in mind that the recovery for this sequence is less than 30 %. The neighbor sites (912, 911) – with nearly full recovery – from deeper water (~1000 m), however, still show in occasional thin intervals extremely high magnetic susceptibility and natural remanent magnetization (NRM) maxima. Visual inspections of Site 912 indicate that these MS maxima are associated with iron sulfide concretions (i.e. greigite) (Figure 5.4). There are currently two (or three) different chains of arguments possible to explain the enrichment of these Fe sulfide concretions:

Post 2.7 Ma: Within the gas hydrate stability zone (~210 mbsf at Site 910), high concentration gradients of methane in the vicinity of massive accumulation of gas hydrates may have prevented the formation/preservation of greigite (Larrasoana et al. 2007) because the rate of sulphide generation by deep AOM is large enough to drive pyritization reactions to completion. A bottom simulating reflector (BSR) indicative for the base of the gas hydrate stability is tentatively observed at one location (Figure 5.6). High amplitude reflectors below the BSR may indicate the presence of free gas.

Post 2.7 Ma: On the contrary, the absence of substantial dilution of chloride and sodium in the sediments – although analysed at rather low-resolution – indicates that hydrates are not present. Occasional formation of iron sulfide concretions in the neighbor site 912 (and 911) are most likely bound to the present (past) zone of bacterial sulfate reduction. The detection of an upward flux of methane into the zone of no sulfate in all sites (Myhre et al. 1995) indicates that sulfate reduction is driven by anaerobic methane oxidation (AOM).

Assuming a scenario described from the Amazon fan during the Pleistocene/Holocene transition (Kasten et al. 1998), the most likely reason for the preservation of iron sulfide concretions (i.e. greigite) in occasional intervals during the last 2.7 Ma is an abrupt drop in sediment (organic carbon) accumulation rates and thus a prolonged fixation of different redox boundaries and reaction fronts at a particular sediment level. Moreover, the repetition of iron sulphur enrichment throughout the sediment sequence (last 2.7 Ma) is similar to observations

from the Amazon fan (Flood et al 1995) and suggests recurring non-steady-state diagenetic phases during which the zone of AOM remained fixed over a longer time period. Since element enrichments in anoxic sediment section are stable, they are preserved with ongoing sedimentation. In total, 3-4 distinct events of greigite preservation based on MS maxima are observed in Hole 912A over the last ~2.2 Ma whereby the last event occurred ~20 m below the present SMT (Figure 5.4). Assuming a constant glaciomarine sedimentation with rates of 10 cm/kyr throughout the sequence, enrichment of greigite occurred prior to the onset of major glaciations in the circum-Arctic (MIS 6, 12, and the MPT at 0.9-1.0 Ma).

Pre 2.7 Ma: Formation of greigite is observed throughout the entire sediment sequence towards the base of Hole 910C and 911A. Similar to the “glacial” units above, the sediments consist of silty clayey mud, however with significantly less number of dropstones (Myhre et al. 1995). Moreover, sedimentation rates are considerable lower (5-10 cm). The lithological boundary in Hole 910C is consistent with the gas hydrate stability zone at ~210 mbsf. Following the argumentation of Larrasoana et al. (2007), occurrence of greigite below the GHSZ may indicate an ancient gas hydrate system. Particularly, the formation of disseminated gas hydrates associated with high concentration of methane favors the preservation of greigite. With constantly high accumulation and/or low hydrogen sulfide production, the sulfidization reaction at the SMT would not achieve full pyritization, thereby steadily contributing a greigite component to the geological record (Fu et al. 2008). In contrast to rapidly deposited glaciomarine sediments over the last 2.7 Ma where a relatively fast rise of the SMT position leave little time for reductive diagenesis, the prolonged fixation of the SMT and thus gradually upward migration of the redox fronts with constant sedimentation rates have fostered the preservation of greigite.

Early Pliocene seepage: Evidence for hydrocarbon fluid flow prior to 2.7 Ma is provided by stable carbon ($\delta^{13}\text{C}$) analysis of planktic and benthic foraminifera in Hole 910C. Negative $\delta^{13}\text{C}$ excursions are observed during various intervals and may indicate the migration of fluids towards the sea bed (Figure 5.5). Particularly around 4.2 Ma, negative benthic $\delta^{13}\text{C}$ values down to -4 ‰ are associated with sulphide (greigite?) filled shells of foraminifera and recrystallized calcite (gypsum?) grains with nearly barren samples immediately above and below this depth. At ~4.8 Ma, negative benthic $\delta^{13}\text{C}$ values corroborate with planktonic $\delta^{13}\text{C}$ excursion of -2 ‰ implying that the foraminifera incorporated isotopically light carbon released from deeper reservoirs in the overlying water column (Rathburn et al. 2003). Bottom water warming and melting of gas hydrates as suggested for the Late Quaternary negative $\delta^{13}\text{C}$ excursion along the East Greenland margin (Millo et al. 2005) may be excluded since bottom water temperatures inferred from Mg/Ca data remain rather constant (1-3 °C). More likely are a coupling between tectonic (uplift/tilting/re-activation of faults) and climate (rapid sea-level drop at ~4.1 Ma) to explain the leakage of hydrocarbons from deeper reservoirs. This inference is supported by (1) an abrupt change in the hinterland sediment supply as indicated by the cease of fine sands and fresh organic debris supply (Figure 5.2), and (2) the post-depositional greigite formation due to fluid flow as evident from the re-magnetization of the sediments between ~4.2 and the base of Hole 910C (~5.8 Ma). From the presently available data, we speculate that the early Pliocene (~4 Ma) uplift and tilting as described for the NW European margin (Stoker et al. 2005a,b, Praeg et al. 2005) was most likely a regional event in the Atlantic-Arctic gateway region that may have promoted (1) the initial build-up of glacial ice in northern Svalbard/Barents Sea and (2) the leakage of deeper reservoirs prior to the onset of large-scale glacial erosion in the Barents Sea. The data indicate that Pleistocene erosion and uplift in the Barents Sea region had probably only minor effects on reservoir leakages than previously thought.

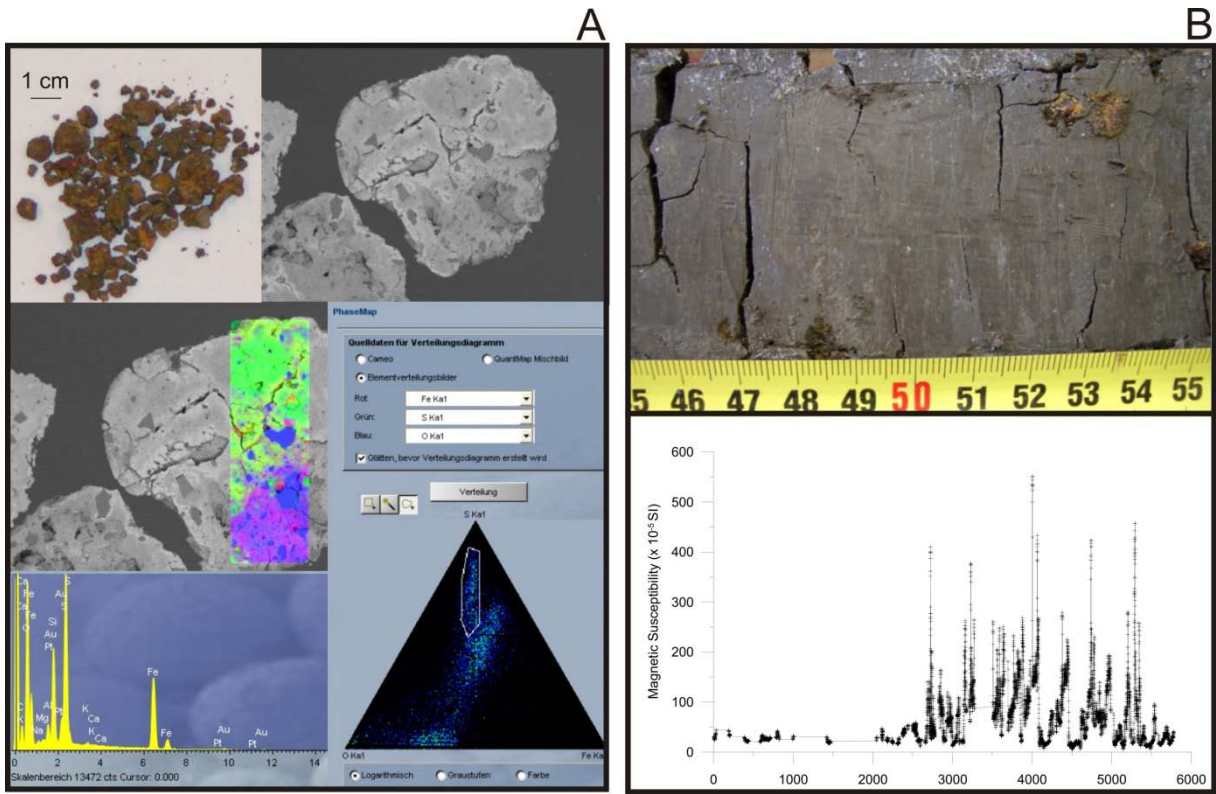


Figure 5.3 (A) Mineral characterization of greigite by SEM and EDX. (B) ODP Hole 910C core photo with greigite (G) concretions and magnetic susceptibility record for the last 6 Myr.

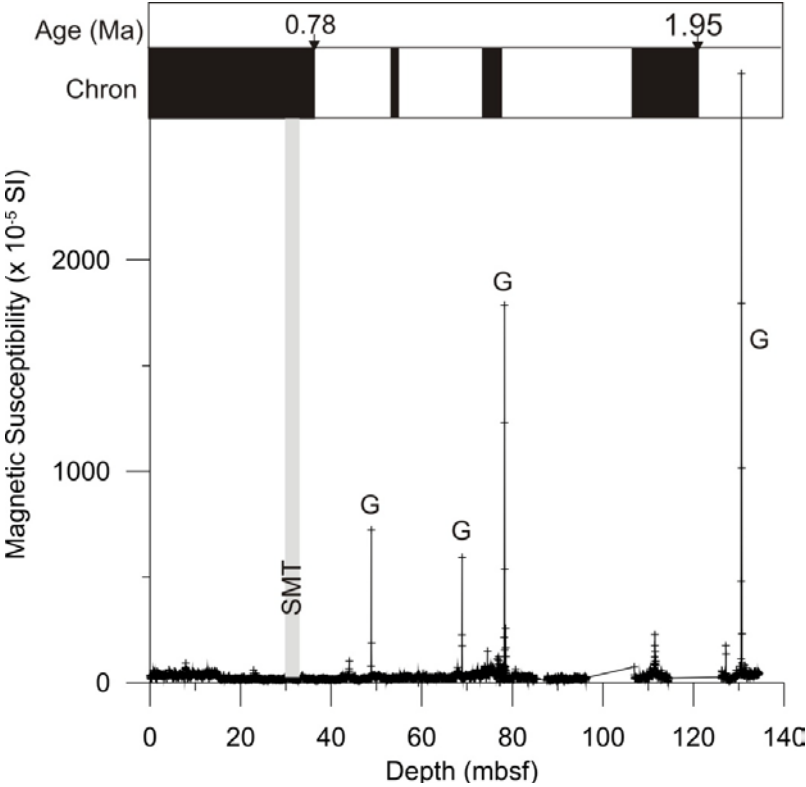


Figure 5.4 Magnetic susceptibility (MS) record of Hole 912A vs. depth. MS maxima are due to greigite (G) preservation. Paleomagnetic (sub-) chrons and respective ages are indicated.

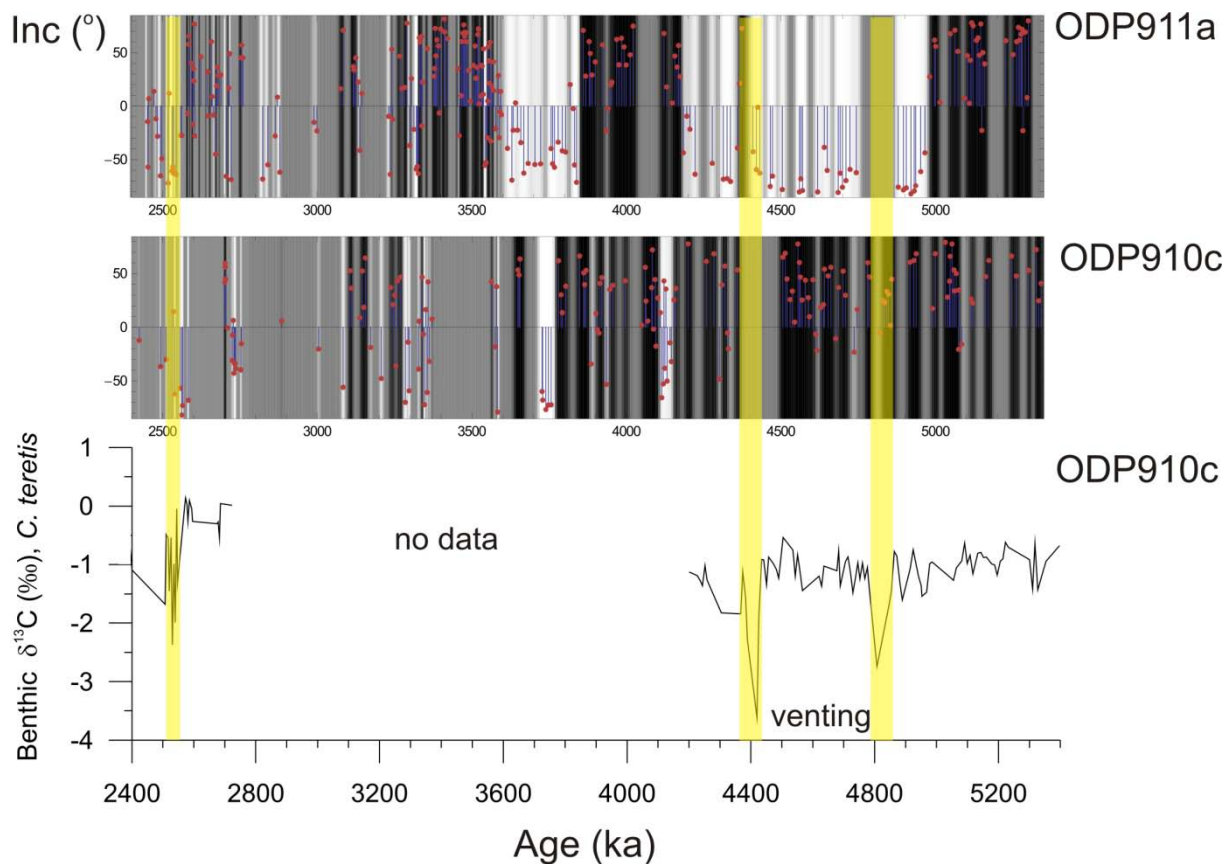


Figure 5.5 Stable benthic carbon isotope record of ODP910C and paleomagnetic inclination of ODP910C and ODP911A on a common approximate age scale. Negative isotope excursions are marked in yellow.

Highlights Module 3: Depositional Environment and hydrocarbon indicators

Depositional Environment

On the southern Yermak Plateau a system of time-migrating anticlines with a semi-parallel reflection pattern, oldest to the west and youngest to the east, dominates the penetrated seismic section (Fig. 3.5.2). This is interpreted as an eastward migrating contourite deposit. The deposition rate through time has generally been higher on the crest and the eastern side than the western side of the plateau (Fig. 3.5.2). This is probably due to higher current velocities on the western side associated with the northern branch of the North Atlantic Current. Units with sub-parallel reflection pattern, characterizing much of the northwestern Svalbard continental margin (Fig. 3.5.3), are also interpreted as contourite deposits. These contourites, where not disturbed by other processes, seem continuous throughout the studied 6 myr period, and also for most of the deeper seismic reflections (Fig. 3.5.2 and Fig. 3.5.3). Several places along the studied NW Svalbard margin the continuous parallel reflection pattern of the contourite deposits are interrupted by thick lens-shaped units with chaotic reflection patterns, interpreted as glacial debris-flow fans (Fig. 3.5.3 & 2.1). Two of these fans, the Isfjorden Fan and Sjubrebanken Fan, started to build up at ~2.7 Ma. The third fan, the Kongsfjorden Fan, started building up at around 1.5 Ma, at the same time as the sediment deposition of the Sjubrebanken Fan dropped dramatically (Fig. 3.5.3). This shift of depocenter, from the Sjubrebanken- to the Kongsfjorden Fan, is probably related to a switch in the location of the sediment source, the ice stream flowing out Kongsfjorden, at around 1.5

Ma. The only location along the western Svalbard margin not affected by glacial fans, is the area between the Kongsfjorden- and Isfjorden fans outside Prins Karls Forland. Here, continuous contouritic sedimentation took place throughout and before the glaciations, which started at ~2.7 Ma. Fig. 3.5.2 shows that at least before ~2 Ma, and probably up to ~1.5 Ma, the Yermak Plateau was a ridge rather than a plateau. The flat plateau of today is a result of erosion leveling off the previous ridge, starting at around 1.5 Ma. The erosion has mostly affected the eastern side and the crest of the plateau, extending down to depths of ~900 m below sea level. 1.5 Ma also marks the time when deep iceberg plough marks on both the eastern and western slope of the Yermak Plateau occur for the first time, probably indicating a major glacial event at this time.

Hydrocarbon indicators

There is ample evidence of hydrocarbon indications on the southern Yermak Plateau (Figs. 5.6 and 5.7). The crestal parts of the eastward migrating anticlines are related to bright-spots with masking below (Figure 5.6A). Many bright-spots are also present in the vicinity of faults, which several places are associated with the anticlines. These bright-spots are probably related to free-gas, migrating up along the faults and permeable layers, accumulating in the structural traps of the anticlines. A possible flat-spot has also been identified on one of the anticlines (Figure 5.6B). In the south and south-eastern part of the Yermak Plateau, two separate sedimentary wedges, interpreted as glacial debris-flow fans, onlap the plateau (Figure 5.7 and Fig. 3.5.2). A series of high-amplitude seismic reflections appear where these fans onlap the plateau (Figure 5.7C and Figure 5.7D). Such high-amplitude reflections are also present where one of the fans downlaps the continental slope outside Kongsfjordrenna (Figure 5.7B). These high-amplitude reflections probably reflect free-gas trapped by the low-permeable debris-flow deposits of the glacial fans.

Potential gas hydrates

Gas hydrates have been described just south of the Yermak Plateau along much of the Western Svalbard margin based on the appearance of seismic bottom simulating reflectors (BSR), reflecting the base of the gas hydrate stability zone (GHSZ). No obvious BSR is present on the seismic profile across the Yermak Plateau (Figure 5.6), but a clear gas hydrate BSR would not be easily recognizable in this area since many of the sedimentary sequences are subparallel to the GHSZ. Calculation of the depth of the base of the GHSZ across the Yermak Plateau (Figure 5.8), however, indicates at least one location with free gas at the base of the GHSZ if we assume the presence of higher component hydrocarbon gases (Figure 5.8 inset). This could imply migration of thermogenic hydrocarbons from deeper petroleum sources.

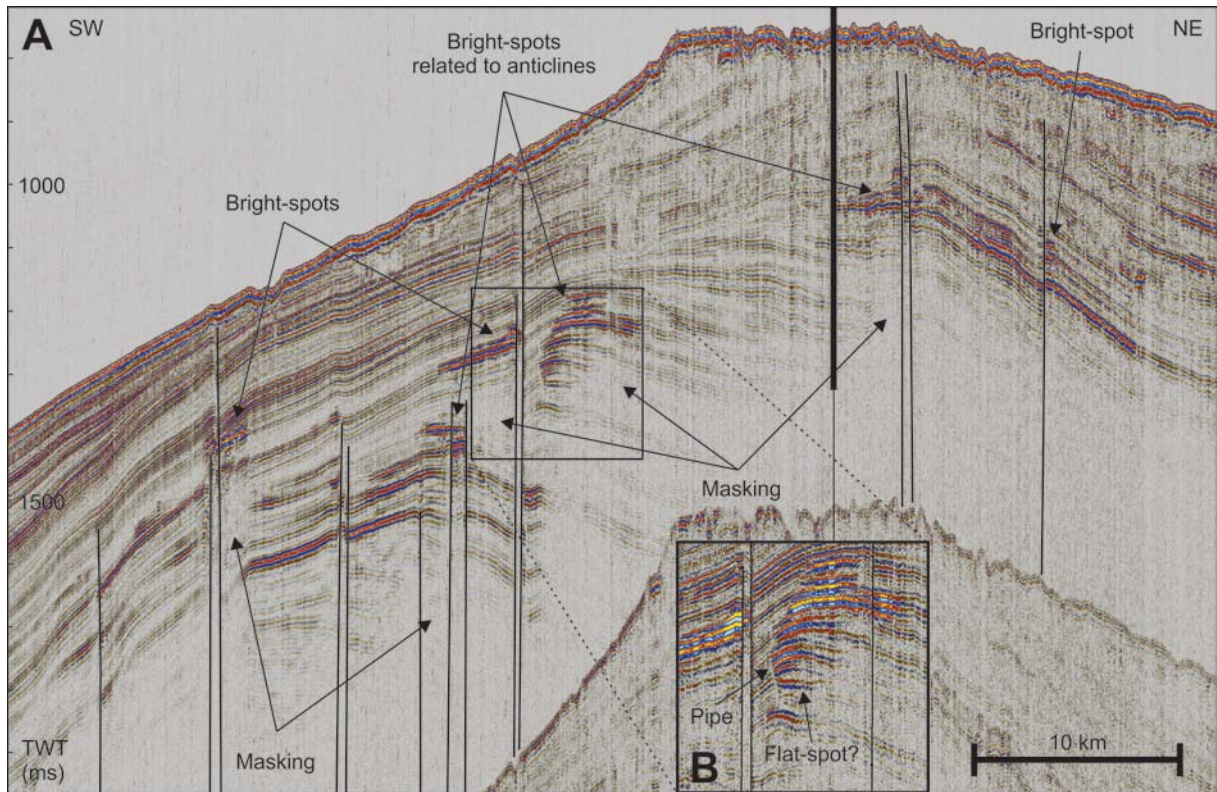


Figure 5.6 (A) Hydrocarbon indications on the Yermak Plateau. (B) Possible flat-spot.

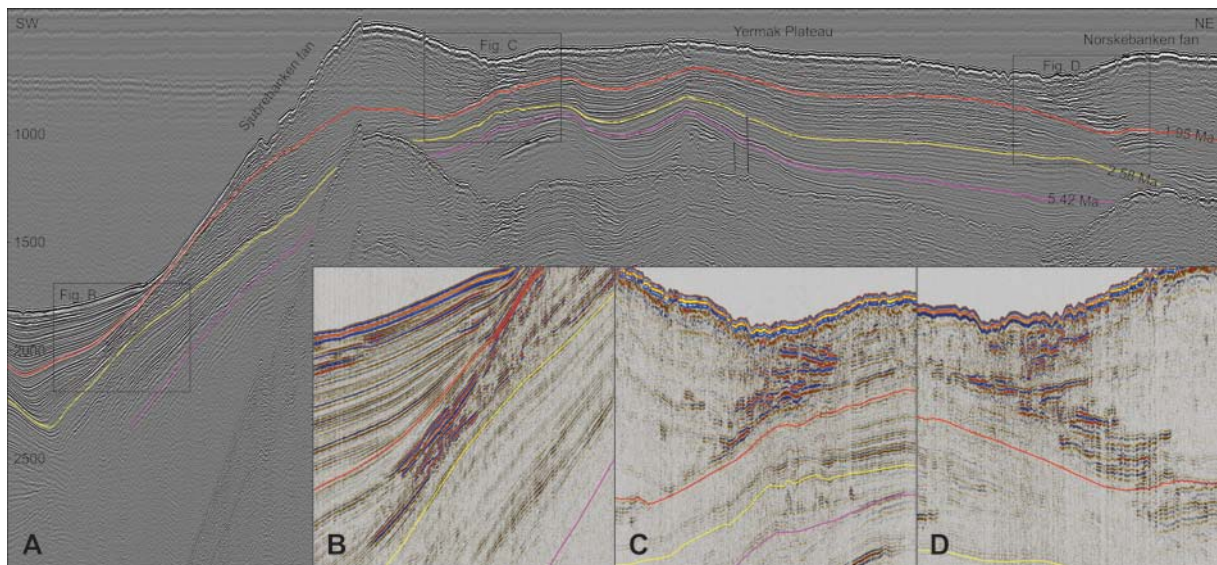


Figure 5.7 (A) Seismic section across the southern parts of the Yermak Plateau crossing the Sjubrebanken fan and parts of the Norskebanken fan. (B) High-amplitude anomalies where the Sjubrebanken fan downlaps on the slope outside Kongsfjorden. (C, D) High-amplitude anomalies located where both the Sjubrebanken- and Norskebanken fans onlap the Yermak Plateau

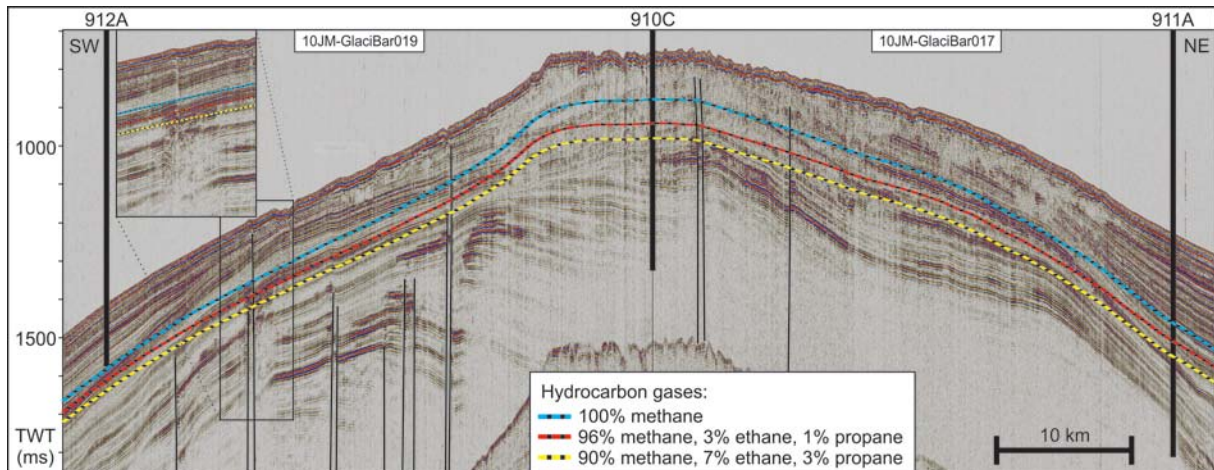


Figure 5.8 Gas hydrate stability zone modeling based on different hydrocarbon gases. Phase equilibrium of hydrates is calculated using the Hydrate Prediction Program (Sloan, 1998). Calculations are done assuming fresh-water in the pore space. Thermal heat gradients are based on measurements from the three ODP wells. 912A = 0.1166 C/m, 910C = 0.0973 C/m, 911A = 0.0795 C/m. Pressures at depth are calculated using an average sediment density of 1900 kg/m³.

6. MAIN CONCLUSIONS

6.1 Stratigraphy:

- Depth-to-depth correlation of new seismic data confirm that Hole 910C has recovered older sediments than Hole 911A.
- Consistent biostratigraphic and paleomagnetic data reveal a base age of Hole 911A close to the Miocene-Pliocene boundary (~5.3 Ma).
- Biostratigraphic data coupled to new stable oxygen and carbon isotope data suggest a Late Miocene age for the base of Hole 910C (~5.8 Ma).
- With our new seismo-stratigraphic framework, we confirm the age of the key seismic reflectors R3 (0.78 Ma), R5 (1.5 Ma), and R7 (2.7 Ma).
- The new Plio-Pleistocene seismo-stratigraphic framework has been established along the western Svalbard margin between the Yermak Plateau and ODP site 986 offshore SW Svalbard.

6.2 Environment:

- The planktic and benthic foraminifera belong to a subpolar – polar fauna from the outer shelf – upper slope. Changes of the fauna assemblages indicate periods of relative changes of the inflow of Atlantic water and sea-ice distribution through the Late Miocene – Pliocene.
- Palynological studies reveal a near-coastal environment and proximity to river outflow during the late Miocene-early Pliocene. Sediment supply from the uplifted, vegetated Barents Sea region dominated the depositional environment during the late Miocene. Frequent pulses of glacially eroded material from northern Svalbard reached the Yermak Plateau since ~4 Ma.
- We confirm the intensification of the Northern Hemisphere Glaciation at ~2.7 Ma (shelf edge glaciations) by abrupt pulses of ice rafted debris on the Yermak Plateau. However, large-scale glaciations covering the entire Barents Sea were not established before ~1.5 Ma.

6.3 Hydrocarbons

- Ample evidence of hydrocarbon accumulations occurs both in seismic and borehole data prior to ~2.7 Ma.
- Post-depositional formation of greigite associated with negative planktic and benthic $\delta^{13}\text{C}$ excursions at ~4 Ma indicate a major fluid flow event.
- A regional uplift event (and fault re-activation) during the early Pliocene along the entire NW European margin including Svalbard associated with a rapid sea level drop may be the ultimate trigger for the fluid flow event at ~4 Ma.
- We speculate whether Pleistocene erosion and uplift in the Barents Sea region had less effect on reservoir leakage than previously thought. Hydrocarbon indications younger than 2.7 Ma are largely absent in both seismic and borehole data.

7. OUTLOOK: CORRELATION POTENTIAL TOWARDS THE SW BARENTS SEA

We have in the seismic correlation of this project focused on establishing a seismo-stratigraphic framework for the continental margin margins north-west and west of Svalbard, between ODP sites 910, 911 and 912 on the Yermak Plateau and site 986 off south-western Svalbard. The reason for this is partly because the seismic correlation north- and west of Svalbard has been challenging and time consuming, taking the time of the PhD working with seismic stratigraphy. This is, however, also due to lack of access to existing Russian seismic data offshore south-western Svalbard (Fig. 3.5.1, maps revealing the UiT database (the green and light brown lines are from MAGE, only the brown have been available for this study)).

Since UiT has managed to get access to seismic MAGE data for the area just south of Svalbard, (Fig. 3.5.1B; light brown lines), we are optimistic with respect to also getting access to their seismic offshore south-western Svalbard during the course of the new NFR *GlaciBar PetroMaks* project (which is the continuation of the Arctic Chronology Project). This would make it possible to extend this new seismo-stratigraphic framework farther southwards and into the SW Barents Sea.

8. REFERENCES

- Anthonissen, E. D. 2008. Late Pliocene and Pleistocene biostratigraphy of the Nordic Atlantic region. *Newsletters on Stratigraphy*, 43, 33-48.
- Bé, A.W.H., and Tolderlund, O.L. (1971) Distribution and ecology of living planktonic foraminifera in surface waters of the Atlantic and Indian Oceans. In Funnell, B.M., and Riedel, W.R. (ed.) *Micropaleontology of Oceans*, Cambridge University Press, London, 105-149.
- Dahlgren, K. I. T., Vorren, T. O., Stoker, M. S., Nielsen, T., Nygard, A., and Sejrup, H. P., 2005. Late Cenozoic prograding wedges on the NW European continental margin: their formation and relationship to tectonics and climate: *Marine and Petroleum Geology*, v. 22, no. 9-10, p. 1089-1110.
- Eidvin, T. And Rundberg, Y. 2001. Late Cainozoic stratigraphy of the Tampen area (Snorre and Visund fields) in the northern North Sea, with emphasis on the chronology of early Neogene Sands. *Norwegian Journal of Geology*, 81, 119-161.
- Faleide, J.I., Solheim, A., Fiedler, A., Hjelstuen, B.O., Andersen, E.S., Vanneste, K., 1996. Late Cenozoic evolution of the western Barents Sea – Svalbard continental margin. *Global and Planetary Change*, v. 12, p. 53-74.
- Feyling-Hanssen, R. W. 1986. Grænsen mellem Tertiær og Kvartær i Nordsøen og Arktis, fastlagt og korreleret ved hjælp af benthoniske foraminiferer. *Dansk Geologisk Forenings Årsskrift for 1985*, 19-33.
- Flood R. D. et al. 1995. *Proc. ODP, Initial Reports, Vol. 155. Ocean Drilling Program, College Station (TX)*.
- Fu, Y. Z., von Dobeneck, T., Franke, C., Heslop, D., and Kasten, S., 2008. Rock magnetic identification and geochemical process models of greigite formation in Quaternary marine sediments from the Gulf of Mexico (IODP Hole U1319A): *Earth and Planetary Science Letters*, v. 275, no. 3-4, p. 233-245.
- Hodell, D. A., Curtis, J. H., Sierro, F. J., and Raymo, M. E., 2001. Correlation of late Miocene to early Pliocene sequences between the Mediterranean and North Atlantic: *Paleoceanography*, v. 16, no. 2, p. 164-178.
- Hald, M. and Steinsund, P. I. 1996. Benthic foraminifera and carbonate dissolution in surface sediments of the Barents- and Kara Seas. In Stein, R., Ivanov, G.I., Levitan, M.A. & Fahl, K., (eds.): *Surface sediment composition and sedimentary processes in the central Arctic Ocean and along the Eurasian Continental Margin. Berichte zur Polarforschung* 212, 285-307.
- International Commission Stratigraphy, 2010. <http://www.stratigraphy.org>.
- Jennings, A. E., Weiner, N. J., Helgadottir, G., and Andrews, J. T. 2004. Modern foraminiferal faunas of the southwestern to northern Iceland shelf: Oceanographic and environmental controls. *Journal of Foraminiferal Research* 34, 180-207.
- Jorissen, F.J., Barmawidjaja, D.M., Puskaric, S., Vanderzwaan, G.J., 1992. Vertical-Distribution of Benthic Foraminifera in the Northern Adriatic Sea - the Relation with the Organic Flux. *Marine Micropaleontology* 19, 131-146.
- Kasten, S., Freudenthal, T., Gingele, F. X., and Schulz, H. D., 1998. Simultaneous formation of iron-rich layers at different redox boundaries in sediments of the Amazon deep-sea fan: *Geochimica Et Cosmochimica Acta*, v. 62, no. 13, p. 2253-2264.
- Kennett, J. P. and Srinivasan, M. S. 1983. *Neogene Planktonic Foraminifera: A phylogenetic atlas*. Hutchinson Ross Publishing Company, 265 p.
- King, C. 1983. *Cainozoic micropaleontological biostratigraphy of the North Sea. Report of the Institute of Geological Sciences* 82-7. London, 40 p.

- Knies, J., Matthiessen, J., Mackensen, A., Stein, R., Vogt, C., Frederichs, T., and Nam, S. I., 2007, Effects of Arctic freshwater forcing on thermohaline circulation during the Pleistocene: *Geology*, v. 35, no. 12, p. 1075-1078.
- Knies, J., Matthiessen, J., Vogt, C., Laberg, J.S., Hjelstuen, B.O., Smelror, M., Larsen, E., Andreassen, K., Eidvin, T. and Vorren, T.O. 2009. The Pliocene glaciation of the Barents Sea-Svalbard region: a new model based on revised chronostratigraphy. *Quaternary Science Reviews* 28, 812-829.
- Korsun, S.A., Polyak, L., 1989. Distribution of benthic foraminiferal morphogroups in the Barents Sea. *Oceanology* 29, 838-844.
- Kristjansdottir, G. B., Lea, D. W., Jennings, A. E., Pak, D. K., and Belanger, C., 2007, New spatial Mg/Ca-temperature calibrations for three Arctic, benthic foraminifera and reconstruction of north Iceland shelf temperature for the past 4000 years: *Geochemistry Geophysics Geosystems*, v. 8.
- Laberg, J. S., Andreassen, K., Knies, J., Vorren, T. O., and Winsborrow, M., 2010, Late Pliocene-Pleistocene development of the Barents Sea Ice Sheet: *Geology*, v. 38, no. 2, p. 107-110.
- Laberg, J. S., Andreassen, K., and Vorren, T. O., 2012, Late Cenozoic erosion of the high-latitude southwestern Barents Sea shelf revisited: *Geological Society of America Bulletin*, v. 124, no. 1-2, p. 77-88.
- Larrasoana, J. C., Roberts, A. P., Musgrave, R. J., Gracia, E., Pinero, E., Vega, M., and Martinez-Rulz, F., 2007, Diagenetic formation of greigite and pyrrhotite in gas hydrate marine sedimentary systems: *Earth and Planetary Science Letters*, v. 261, no. 3-4, p. 350-366.
- Lisiecki, L. E., and Raymo, M. E., 2005, A Pliocene-Pleistocene stack of 57 globally distributed benthic delta O-18 records: *Paleoceanography*, v. 20, no. 1.
- Loeblich, A.R., and Tappan, H., 1988. *Foraminiferal Genera and Their Classification* (Vol. 1 and 2): New York (Van Nostrand Reinhold Co.).
- Lourens, L.J., Hilgen, F.J., Shackleton, N.J., Laskar, J., and Wilson, D., 2004. The Neogene Period. In Gradstein, F.M., Ogg, J.G., Smith, A.G. (Eds.), *A Geological Time Scale*: Cambridge Univ. Press, 409-440.
- Mackensen, A., Hald, M., 1988. *Cassidulina teretis* Tappan and *C. laevigata* d'Orbigny; their modern and late Quaternary distribution in northern seas. *Journal Of Foraminiferal Research* 18, 16-24.
- Millo, C., Sarnthein, M., Erlenkeuser, H., and Frederichs, T., 2005, Methane-driven late Pleistocene delta C-13 minima and overflow reversals in the southwestern Greenland Sea: *Geology*, v. 33, no. 11, p. 873-876.
- Myhre, A.M., Thiede, J., Firth, J.V., et al., 1995. *Proceedings of the Ocean Drilling Program, Initial Reports*, v. 151. College Station, TX.
- Oda, H., Torii, M., 2004. Sea-level change and remagnetization of continental shelf sediments off New Jersey (ODP Leg 174a): Magnetite and greigite diagenesis. *Geophysical Journal International*, 156, 443-458.
- Ogg, J.G., Ogg, G. and Gradstein, F.M. 2008. *The Concise Geologic Time scale*. Cambridge University Press, 150 pp.
- Ottesen, R.T., Bogen, J., Finne, T.E., Andersson, M., Dallmann, W.K., Eggen, O.A., Jartun, M., Lundkvist, Q., Pedersen, H.R., Volden, T. 2010: *Geochemical Atlas of Norway. Part 2: Geochemical atlas of Spisbergen – Chemical composition of overbank sediments*. Geological Survey of Norway, Trondheim, Norway, 160pp.
- Praeg, D., Stoker, M. S., Shannon, P. M., Ceramicola, S., Hjelstuen, B., Laberg, J. S., and Mathiesen, A., 2005, Episodic Cenozoic tectonism and the development of the NW

- European 'passive' continental margin: *Marine and Petroleum Geology*, v. 22, no. 9-10, p. 1007-1030.
- Rathburn, A. E., Perez, M. E., Martin, J. B., Day, S. A., Mahn, C., Gieskes, J., Ziebis, W., Williams, D., and Bahls, A., 2003, Relationships between the distribution and stable isotopic composition of living benthic foraminifera and cold methane seep biogeochemistry in Monterey Bay, California: *Geochemistry Geophysics Geosystems*, v. 4.
- Schafstall, N. 2011. The pollen records from ODP Hole 910C and 911A near Svalbard. Ms thesis, Utrecht University, The Netherlands, 13pp.
- Spezzaferri, S., 1998. Planktonic foraminifer biostratigraphy and paleoenvironmental implications of Leg 152 sites (East Greenland Margin). In Saunders, A.D., Larsen, H.C., and Wise, S.W., Jr. (Eds.), *Proc. ODP, Sci. Results, 152*: College Station, TX (Ocean Drilling Program), 161–189.
- Stoker, M. S., Hout, R. J., Nielsen, T., Hjelstuen, B. O., Laberg, J. S., Shannon, P. M., Praeg, D., Mathiesen, A., van Weering, T. C. E., and McDonnell, A., 2005. Sedimentary and oceanographic responses to early Neogene compression on the NW European margin: *Marine and Petroleum Geology*, v. 22, no. 9-10, p. 1031-1044.
- Stoker, M. S., Praeg, D., Hjelstuen, B. O., Laberg, J. S., Nielsen, T., and Shannon, P. M., 2005. Neogene stratigraphy and the sedimentary and oceanographic development of the NW European Atlantic margin: *Marine and Petroleum Geology*, v. 22, no. 9-10, p. 977-1005.
- van Voorthuysen, J. H. 1950. The quantitative distribution of the Pleistocene, Pliocene and Miocene Foraminifera of boring Zaandam (Netherlands). *Mededelingen Geologische Stichting, Nieuwe Serie*, 4, 51-72.
- Verhoeven, K. and Louwye, S. 2011. *Selenopemphix islandensis* sp. nov.: a new organic-walled dinoflagellate cyst from the Lower Pliocene Tjörnes beds, northern Iceland. *Palynology*, doi: 0.1080/01916122.2011.593573.
- Weaver, P. P. E. and Clement, B. M. 1987. Magentobiostratigraphy of planktonic foraminiferal datums. In: Ruddiman, W. F., Kidd, R. B., Thomas, E. (eds.), *Init Repts DSDP, 94*. Washington, 815-829.
- Willard, D.A. 1996. Pliocene-Pleistocene pollen assemblages from the Yermak Plateau, Arctic Ocean: Sites 910 and 911. In: Thiede, J., Myhre, A.M., Firth J.V., Johnson, G.L., Ruddiman, W.F. (eds.), *Proc. ODP Scientific Results, 151*. College Station, TX (Ocean Drilling Program), 297-305.
- Zachos, J., Pagani, M., Sloan, L., Thomas, E., and Billups, K., 2001. Trends, rhythms, and aberrations in global climate 65 Ma to present: *Science*, v. 292, no. 5517, p. 686-693.